농 학 박 사 학 위 논 문

Structural basis for a cofactor-dependent oxidation protection and catalysis of cyanobacterial SSADH

시아노박테리아 succinic semialdehyde dehydrogenase의 조효소를 이용한 산화방지와 구조 및 기능에 대한 연구.

2014년 2월

서울대학교 대학원
농생명공학부 응용생명화학전공
박 진 서

Thesis of the Degree of Doctor of Philosophy

Structural basis for a cofactor-dependent oxidation protection and catalysis of cyanobacterial SSADH

Advisor : Sangkee Rhee

Jinseo Park

February 2014

Structural basis for a cofactor-dependent oxidation protection and catalysis of cyanobacterial SSADH

시아노박테리아 succinic semialdehyde dehydrogenase의 조효소를 이용한 산화방지와 구조 및 기능에 대한 연구.

지도교수: 이 상 기

이 논문을 농학박사학위논문으로 제출함
2014 년 1 월

서울대학교 대학원
농생명공학부 응용생명화학전공
박 진 서

박진서의 박사학위논문을 인준함
2014 년 1 월

위 원 장 _____

부위원장 _____

위 원 _____

위 원 _____

위 원 _____

Structural basis for a cofactor-dependent oxidation protection and catalysis of cyanobacterial SSADH

Advisor : Sangkee Rhee

A dissertation submitted in partial fulfillment
of the requirement for the degree of

DOCTOR OF PHILOSOPHY

to the Faculty of
Department of Agricultural Biotechnology
at

SEOUL NATIONAL UNIVERSITY

by

Jinseo Park

Date Approved

_____

_____

_____

_____

_____

_____

ABSTRACT

Succinic semialdehyde dehydrogenase (SSADH) from cyanobacterium *Synechococcus* belongs to aldehyde dehydrogenase (ALDH) superfamily. The structure features and functional details for members of ALDH family were well established. The main functional role of the ALDH family is to convert an aldehyde group of substrate to a carboxyl group. In spite of low sequence identity among the members, enzymes in the family exhibit structural similarites and highly conserved catalytic loops including the catalytic cysteine and glutamate residues. SSADHs as a member of the γ-aminobutyrate shunt produce succinate through the oxidation of an aldehyde group in succinic semialdehyde which serves as an intermediate of γ-aminobutyrate degradation. But *Synechococcus* SSADH (SySSADH) differs from other SSADHs in the γ-aminobutyrate shunt. SySSADH is a TCA cycle enzyme and completes a 2-oxoglutarate dehydrogenase-deficient cyanobacterial TCA cycle through a detour metabolic pathway. SySSADH produces succinate in an $NADP^+$-dependent manner with a single cysteine acting as the catalytic residue in the catalytic loop. Crystal structures of SySSADH were determined in its apo form, as a binary complex with $NADP^+$, and as a ternary complex with succinic semialdehyde and NADPH, providing details about the catalytic mechanism by revealing a covalent adduct of a cofactor with the catalytic cysteine in the binary complex and a proposed thiohemiacetal intermediate in the ternary complex. Further analyses showed that SySSADH is an oxidation-sensitive enzyme and that the formation of the NADP–cysteine adduct is a kinetically preferred event that

protects the catalytic cysteine from H_2O_2-dependent oxidative stress. These structural and functional features of SySSADH provide a molecular basis for cofactor-dependent oxidation protection in 1-Cys SSADH, which is unique relative to other 2-Cys SSADHs employing a redox-dependent formation of a disulfide bridge.

Key words; Aldehyde dehydrogenase, Oxidation protection, Cofactor, Succinic semialdehyde dehydrogenase, *Synechococcus* sp. PCC 7002, Tricarboxylic acid cycle

Student Number; 2009-30309

CONTENTS

LIST OF FIGURES

LIST OF TABLES

LIST OF ABBREVIATIONS

SSADH	succinic semialdehyde dehydrogenase
SSA	succinic semialdehyde
GABA	γ-aminobutyrate
TCA	tricarboxylic acid
ALDH	aldehyde dehydrogenase
HsSSADH	human SSADH
EcSSADH	*Escherichia coli* SSADH
SySSADH	SSADH from *Synechococcus* sp. PCC 7002
SeMet	seleno-L-methionine
RMSD	root mean-square deviation.

1. Introduction

Succinic semialdehyde dehydrogenase (SSADH) from cyanobacterium *Synechococcus* belongs to aldehyde dehydrogenase (ALDH) superfamily (1, 2). The main functional role for members of the ALDH family is to convert an aldehyde group of substrate to a carboxyl group. In alcohol metabolism, structure and mechanism of acetalaldehyde dehydrogenase in the ALDH family were well established and it oxidizes acetaldehyde to acetic acid with an NAD^+ as a cofactor (3) (Figure 1*A*). Despite of low sequence identity among members of the family, the structural features and the identity of the residues consisting of the active site were highly conserved in the family, including a cysteine and a glutamate residue acting as a catalytic residue and a general base, respectively (4).

An $NAD(P)^+$-dependent SSADH (EC 1.2.1.79)[2] as a member of γ-aminobutyrate (GABA) shunt catalyzes succinic semialdehyde (SSA) into its corresponding acid, succinate via the oxidation of an aldehyde group in the substrate (Figure 1*B*). SSADHs are ubiquitous in a wide range of organisms, including mammals, plants, and bacteria. In particular, in the mammalian central nervous system, GABA acts as the chief inhibitory neurotransmitter (5). In order to regulate the production of GABA, mitochondrial SSADH plays a crucial role in the GABA degradation pathway (6, 7) where it is responsible for the final reaction in the shunt and thus provides the carbon contained in GABA as a form of succinate to the ATP-generating tricarboxylic acid (TCA) cycle. Mutation-induced malfunction or a deficiency in SSADH activity causes the accumulation of SSA, the final intermediate of the GABA degradation pathway, and then SSA is reduced to γ-hydroxybutyric acid by γ-hydroxybutyric dehydrogenase (8). The elevation of γ-

hydroxybutyric acid has attributed to an uncommon and heritable neuropharmacological disorder in humans (9). Similar deficiencies in plants cause various developmental and phenotypic changes (10, 11).

Similar to the role of human and plant SSADH in secondary metabolism, bacterial SSADH plays an important role in carbon and nitrogen metabolism (12). Recently, SSADH was recognized to play a novel role in the primary metabolic pathway of cyanobacteria. The TCA cycle in cyanobacteria has long been considered incomplete, mainly due to a lack of 2-oxoglutarate dehydrogenase, an enzyme that catalyzes the conversion of 2-oxoglutarate to succinyl-CoA (13). However, the recent identification of two different genes for 2-oxoglutarate decarboxylase and SSADH from *Synechococcus* sp. PCC 7002 indicates that the TCA cycle in *Synechococcus* bypasses the production of succinyl-CoA and produces succinate from 2-oxoglutarate via SSA using these two enzymes (Figure 2) (14). Therefore, cyanobacterial 2-oxoglutarate decarboxylase and SSADH act as members of the TCA cycle by replacing 2-oxoglutarate dehydrogenase and succinyl-CoA synthetase.

SSADH structures in humans (15) and *Escherichia coli* (16, 17) have recently become available. The catalytic cysteine residue of ALDH family is highly susceptible to reactive oxygen species like hydrogen peroxide, and easily oxidized to sulfinic and cysteic acid forms (18). Those investigations highlighted a redox-dependent regulation of SSADH activity. Human SSADH (HsSSADH) contains a catalytic loop with two cysteine residues (2-Cys SSADH), including the catalytic cysteine (Figure 3), which form a reversible disulfide bridge in response to redox conditions. As a result, the loop undergoes a large conformational transition

between a functionally active open form in the reduced state and a catalytically inactive, closed form in the oxidized state (15). In contrast, the structural features of 2-Cys *E. coli* SSADH (EcSSADH) were investigated only in its reduced form (16, 17).

Given the redox-dependent regulation of HsSSADH, the oxidation-resistant catalytic features of *Mycobacterium tuberculosis* SSADH (19), and the ATP-dependent catalytic properties of *Arabidopsis thaliana* SSADH (20), the regulation of SSADH activity is much more complex than initially thought. The different regulatory mechanisms by which these enzymes are controlled remain to be resolved. In particular, a general catalytic mechanism analogous to that of the ALDH family has long been considered (Figure 4) (4, 21). Briefly, a catalytic cysteine carries out a nucleophilic attack on the carbonyl carbon of an incoming SSA, forming a thiohemiacetal intermediate. A thioester intermediate is then formed after a hydride transfer from the proposed intermediate to $NAD(P)^+$. Subsequently, a water molecule activated by a general base carries out a deacylation to produce succinate as a product. Here, I determined, together with a functional analysis. SySSADH is an $NADP^+$-dependent enzyme (14) and differs from HsSSADH and EcSSADH in that it contains only one cysteine in the catalytic loop (1-Cys SSADH), which acts as the catalytic residue (Figure 3). Three different structures of SySSADH were determined, including a 1.7 Å resolution apo structure, a 1.4 Å resolution binary complex with $NADP^+$, and a 1.4 Å resolution ternary complex with SSA and NADPH. Unexpectedly, a covalent adduct of $NADP^+$ was discovered with the catalytic cysteine in the binary complex, as well as the proposed thiohemiacetal intermediate in the ternary complex, with different

conformations of the cofactor in each complex. These results, along with kinetic and functional analyses, provide molecular insights into the cofactor-dependent oxidation protection and mechanistic features of SySSADH.

Figure 1. **Schemes of alcohol metabolism and SSADH catalysis.** *A.* A scheme for alcohol metabolism. *B.* for SSADH catalysis.

A

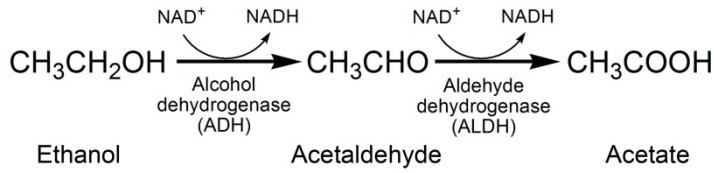
NAD+
NADH
NAD+
NADH
CH3CH2OH
CH3CHO
CH3COOH
Alcohol dehydrogenase (ADH)
Aldehyde dehydrogenase (ALDH)
Ethanol
Acetaldehyde
Acetate

B

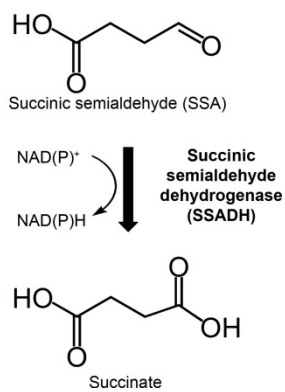
HO
O
O
Succinic semialdehyde (SSA)
NAD(P)+
NAD(P)H
Succinic semialdehyde dehydrogenase (SSADH)
HO
O
O
OH
Succinate

Figure 2. **SySSADH in the cyanobacterial TCA cycle.** A schematic representation of the TCA cycle in cyanobacterium *Synechococcus* is shown with the functional role of SySSADH characterized in the cycle.

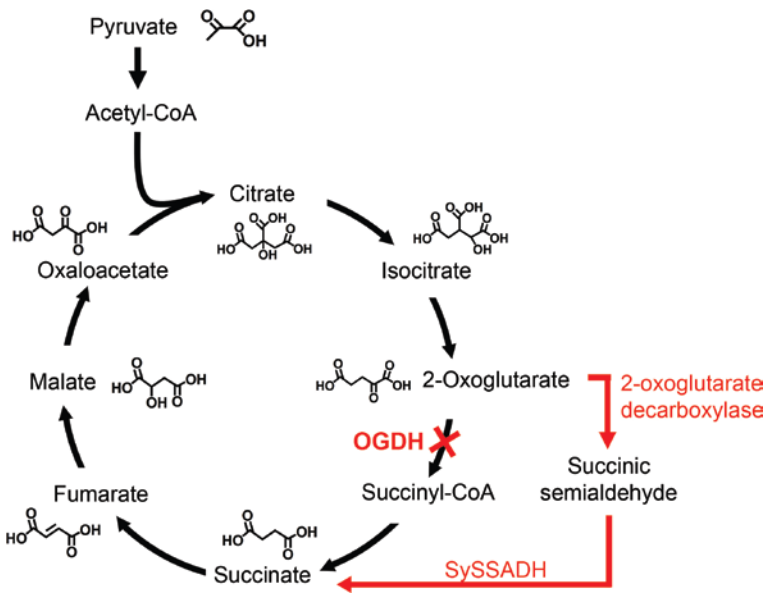
Pyruvate
Acetyl-CoA
Citrate
Oxaloacetate
Isocitrate
Malate
2-Oxoglutarate
2-oxoglutarate
decarboxylase
OGDH
Succinic
semialdehyde
Fumarate
Succinyl-CoA
Succinate
SySSADH

Figure 3**. A sequence alignment of SySSADH.** The amino acid sequences of SySSADH are compared with other members of the family, including MtSSADH for *Mycobacterium tuberculosis* SSADH (Gene Accession No. CAB03694), EcSSADH for *E. coli* SSADH (Gene Accession No. NP_417147), AtSSADH for *Arabidopsis thaliana* SSADH (Gene Accession No. NP_178062), and HsSSADH for human SSADH (Gene Accession No. NP_001071). Note that the catalytic loop is boxed in green. EcSSADH, as well as AtSSADH and HsSSADH have two cysteine residues in the loop (2-Cys SSADH), while SySSADH and MtSSADH have a single cysteine for the catalytic residue (1-Cys SSADH). Highly conserved residues are shown in red and boxed in blue. Strictly conserved residues are shown with a red background. Secondary structural elements defined in the apo form of SySSADH are shown for the corresponding SySSADH sequences with the N-, C-, and dimerization domains in magenta, blue, and green, respectively. Red asterisks represent catalytic Cys-262 and the general base Glu-228 in SySSADH. The second cysteine within the catalytic loop is marked with a cyan asterisk. Orange and blue rectangles indicate residues that interact with $NADP^+$ and SSA, respectively. This figure was prepared using ESPript (22).

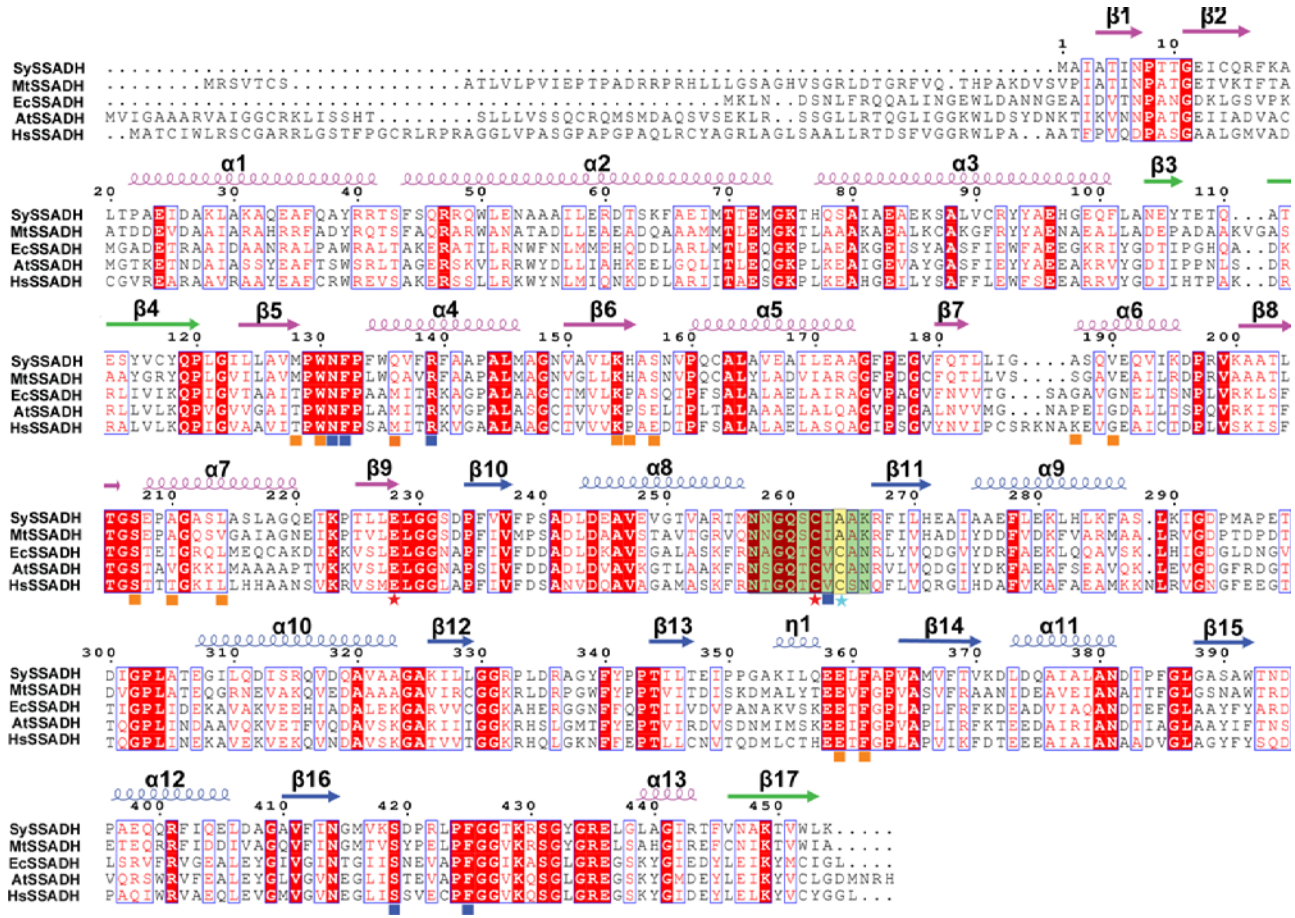
β1
β2
SySSADH
MtSSADH
EcSSADH
AtSSADH
HsSSADH
α1
α2
α3
β3
β4
β5
α4
β6
α5
β7
α6
β8
α7
β9
β10
α8
β11
α9
α10
β12
β13
η1
β14
α11
β15
α12
β16
α13
β17

Figure 4. **A general mechanism of ALDH family.** A general mechanism of ALDH activity is presented with a catalytic cysteine and a general base glutamate.

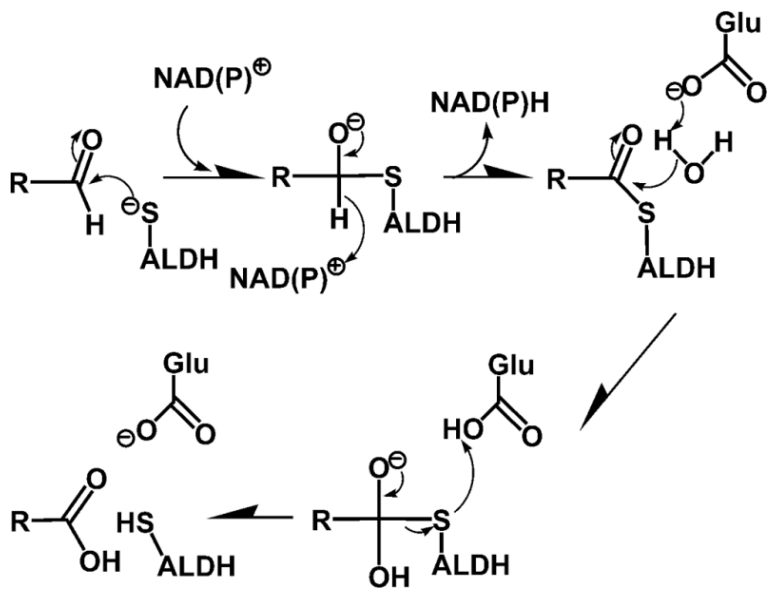
NAD(P)⊕
NAD(P)H
Glu
R
O
H
S
ALDH
NAD(P)⊕
HS
OH

2. Materials and Methods

2.1 Cloning, expression and purification

The gene for SySSADH (GenBank Accession Number NC010475.1) (14) was synthesized from Bioneer (Daejeon, Korea) with codon optimization for expression in *E. coli*. The resulting DNA was restricted by NdeI and XhoI enzymes and subcloned into a modified pET-28a vector (Merck) containing a tobacco etch virus protease cleavage site between the His_5-tag and a multiple cloning site. For structural studies, seleno-L-methionine (SeMet)-substituted, N-terminal His-tagged SySSADH (residues Met-1 to Lys-454) was expressed in *E. coli* B834 (DE3) methionine auxotroph cells (Merck). Cells were grown at 37°C in minimal medium supplemented with SeMet to an OD_{600} of 0.7. The cells were then induced for 16 h at 20°C by the addition of 0.5 mM isopropyl-β-D-thiogalactopyranoside. The cells were harvested and sonicated in buffer A [50 mM HEPES (pH 7.6), 150 mM NaCl, 1 mM DTT]. The enzyme was purified using immobilized metal affinity chromatography with buffer A plus 500 mM imidazole. After the purified SySSADH was dialyzed against buffer A, the N-terminal His-tag was removed by treatment with tobacco etch virus protease for 16 h at 22°C. SySSADH was then further purified by immobilized metal affinity chromatography and size-exclusion chromatography using a Superdex 200 column (GE Healthcare) equilibrated with buffer A. The enzyme was concentrated to 13 mg mL^{-1} based on its molar extinction coefficient of 40,910 M^{-1} cm^{-1} at 280 nm.

2.2 Crystallization

The apo form of SeMet-SySSADH was crystallized at 22°C using the sitting-drop vapor-diffusion method in a crystallization buffer of 0.05 M potassium phosphate monobasic, 20% (w/v) PEG8000, and 2 mM $CaCl_2$ (Figure 5). Formation of the SySSADH–ligand complex, either with $NADP^+$ for the binary complex or NADPH and SSA for the ternary complex, was achieved by soaking the crystal with the cofactor and/or substrate. For the binary complex with $NADP^+$, a pre-grown crystal of SySSADH was soaked for 60 min in a solution of 0.05 M potassium phosphate monobasic, 20% (w/v) PEG8000, 30% (v/v) ethylene glycol, and 50 mM NADPH. An additional 50 mM SSA was included in the soaking solution for the ternary complex. In both experiments, ethylene glycol was used as a cryoprotectant.

Figure 5. **Crystals of SySSADH.** The apo form of SeMet-SySSADH was crystallized in a crystallization buffer of 0.05 M potassium phosphate monobasic, 20% (w/v) PEG8000, and 2 mM $CaCl_2$

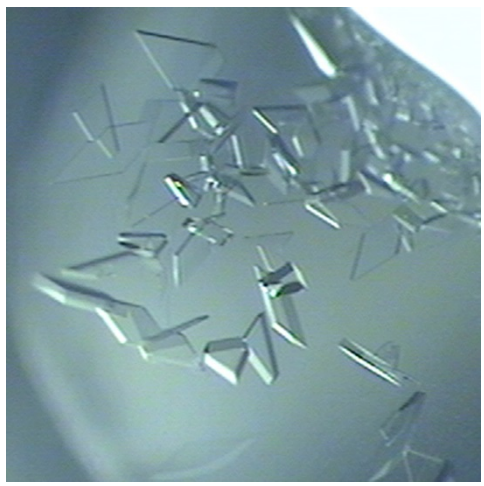

2.3 Data collection and structure determination

Multiwavelength anomalous dispersion data for the apo form of SeMet-SySSADH were collected to a resolution of 1.7 Å on beamline 7A of the Pohang Accelerator Laboratory (Pohang, Korea). Single-wavelength diffraction data to a resolution of 1.4 Å were collected on beamline 5C at the same facility for the binary and the ternary complexes. All data were collected at 100 K and processed using the program HKL2000 (23). The crystals belonged to the space group $P2_12_12_1$, with two monomers per asymmetric unit (Table 1). The structure of SySSADH in its apo form was determined by molecular replacement after failing to locate selenium atoms using single- and multiwavelength anomalous dispersion data. The program PHENIX with an AUTOMR option (24) was used for molecular replacement with PDB ID 3EFV, SSADH from *Salmonella typhimurium* (43% sequence identity; Center for Structural Genomics of Infectious Diseases), as a search model. Manual model building and refinement were performed using the programs COOT (25) and PHENIX, respectively. After several iterative cycles of manual inspection and refinement, the model was built including Ile-3 to Lys-454 for each monomer. The refined apo form was then used as an initial model to solve the structures of the binary and ternary complexes. Structural refinements were performed including a rigid-body refinement followed by simulated annealing and TLS refinement. At the final refinement stage, water molecules, whose refined temperature factors were less than 50 $Å^2$, were assigned based on possible hydrogen bonds to the enzyme or other nearby water molecules. Details regarding data and structural refinement are described in Table 3. Structural comparisons and analyses were carried out using the CCP4 suite program (26). Figures were

prepared using PyMOL (DeLano, W.L., PyMOL Molecular Graphics System, Palo Alto, CA, USA).

Table 1. **Data collection and refinement statistics.**

	Apo	Binary	Ternary
Soaking Condition		50 mM NADPH	50 mM NADPH, SSA
(Soaking time, min)		60	60
Data collection			
Space group	$P2_12_12_1$	$P2_12_12_1$	$P2_12_12_1$
Cell dimensions			
a, *b*, *c* (Å)	42.8, 115.3, 179.3	42.9, 115.5, 180.1	43.0, 115.4, 180.1
Wavelength (Å)	0.97935	0.97948	0.97948
Resolution (Å)	50-1.7	50-1.4	50-1.4
	(1.76-1.70)[a]	(1.45-1.40)	(1.45-1.40)
R_{sym} or R_{merge}[b] (%)	17.4(58.9)	11.0(49.2)	10.5(45.8)
$I / \sigma I$	15.9(4.8)	27.4(5.2)	30.6(5.1)
Completeness (%)	99.5(99.4)	99.7(99.6)	99.9(100.0)
Redundancy	14.3(14.7)	13.9(14.1)	14.5(14.5)
Refinement			
Resolution (Å)	39.1-1.7	41.7-1.4	41.9-1.4
No. unique reflections	98292	176393	176908
R_{work}[c] / R_{free}[d]	18.3 / 20.6	17.5 / 18.7	17.4 / 19.0
No. atoms			
Protein[e]	6882	6882	6892
Ligand[f]	134	232	206
Water	610	690	681
Average *B*-factors			
Protein (Å^2)	13.8	10.8	12.1
Ligand (Å^2)	22.5	18.2	18.5
Water (Å^2)	22.2	19.3	20.5
r.m.s deviations			
Bond lengths (Å)	0.006	0.006	0.006
Bond angles (°)	1.1	1.14	1.12
Ramachandran plot			
Favored (%)	97.7	97.8	98
Allowed (%)	2.2	2	1.8
Disallowed (%)[g]	0.1	0.2	0.2

[a]Numbers in parentheses refer to data in the highest resolution shell.

[b]$R_{merge} = \Sigma|I_h - \langle I_h \rangle| / \Sigma I_h$, where I_h is the observed intensity and $\langle I_h \rangle$ is the average intensity.

[c]$R_{work} = \Sigma ||F_{obs}|-k|F_{cal}|| / \Sigma|F_{obs}|$

[d]R_{free} is the same as R_{work} for a selected subset (10%) of the reflections that was not included in prior refinement calculations.

[e]Ordered residues: the apo structure and the binary complex (Ile-3 to Lys-454 in two monomers) and the ternary complex (Ala-2 to Lys-454 in two monomers).

[f]Ligand: the apo structure (phosphate ion and ethylene glycol), the binaty complex ($NADP^+$ and ethylene glycol), and the ternary complex (NADPH, SSA and ethylene glycol).

[g]Disallowed residues identified using a program Molprobity (27): the apo structure (Gly-386 in one monomer), the binary and ternary complex (Gly-386 in two monomers).

2.4 Dehydrogenase activity assays

Genes for mutant enzymes were prepared by site-directed mutagenesis using a QuikChange Kit (Agilent Technologies) with mutagenic primers (Table 2). All enzymes, including the WT enzyme, were expressed in Luria–Bertani medium using the procedures described above, with the exception of using *E. coli* BL21(DE3) strain as an expression host (Agilent Technologies). The N-terminal His-tagged enzymes were purified in the absence of DTT using immobilized metal affinity chromatography and dialyzed against 50 mM HEPES (pH 7.6). Enzyme assays for the steady-state kinetics were performed at 30°C using a UV-visible spectrophotometer (Jasco). Standard assay solution contained 100 mM HEPES (pH 7.6), 10 mM DTT, 10 mM $CaCl_2$, and 15 μg (153 nM) of SySSADH enzyme. With the addition of 2.5 mM $NADP^+$, the reaction mixture was incubated for 10 min at 30°C. The reaction was then initiated by the addition of 200 μM SSA. Initial velocity was determined by measuring the linear increase in absorbance at 340 nm for the first 30s and calculated as the NADPH concentration produced per minute. The molar extinction coefficient of the solution at 340 nm was 6220 $M^{-1}\,cm^{-1}$. K_m and V_{max} values for $NADP^+$ were calculated using SigmaPlot (Systat Software).

Table 2. **Primer sequences used in this study.**

SySSADH primer				
N131A	Forward	5'-	GCTGTTATGCCGTGG**GCT**TTTCCCTTCTGGCAG	-3'
	Reverse	5'-	CTGCCAGAAGGGAAA**AGC**CCACGGCATAACAGC	-3'
N131D	Forward	5'-	GCTGTTATGCCGTGG**GAT**TTTCCCTTCTGGCAG	-3'
	Reverse	5'-	CTGCCAGAAGGGAAA**ATC**CCACGGCATAACAGC	-3'
F132A	Forward	5'-	GTTATGCCGTGGAAT**GCT**CCCTTCTGGCAGGTC	-3'
	Reverse	5'-	GACCTGCCAGAAGGG**AGC**ATTCCACGGCATAAC	-3'
W135A	Forward	5'-	TGGAATTTTCCCTTC**GCG**CAGGTCTTTCGTTTT	-3'
	Reverse	5'-	AAAACGAAAGACCTG**CGC**GAAGGGAAAATTCCA	-3'
R139A	Forward	5'-	TTCTGGCAGGTCTTT**GCT**TTTGCAGCTCCAGCA	-3'
	Reverse	5'-	TGCTGGAGCTGCAAA**AGC**AAAGACCTGCCAGAA	-3'
R139K	Forward	5'-	TTCTGGCAGGTCTTT**AAA**TTTGCAGCTCCAGCA	-3'
	Reverse	5'-	TGCTGGAGCTGCAAA**TTT**AAAGACCTGCCAGAA	-3'
E228Q	Forward	5'-	AAACCGACTCTGTTG**CAA**CTGGGTGGCTCAGAT	-3'
	Reverse	5'-	ATCTGAGCCACCCAG**TTG**CAACAGAGTCGGTTT	-3'
E228A	Forward	5'-	AAACCGACTCTGTTG**GCA**CTGGGTGGCTCAGAT	-3'
	Reverse	5'-	ATCTGAGCCACCCAG**TGC**CAACAGAGTCGGTTT	-3'
C262A	Forward	5'-	AACAACGGTCAGTCT**GCT**ATTGCGGCTAAGAGA	-3'
	Reverse	5'-	TCTCTTAGCCGCAAT**AGC**AGACTGACCGTTGTT	-3'
I263A	Forward	5'-	AACGGTCAGTCTTGT**GCT**GCGGCTAAGAGATTT	-3'
	Reverse	5'-	AAATCTCTTAGCCGC**AGC**ACAAGACTGACCGTT	-3'
S419A	Forward	5'-	AACGGTATGGTGAAA**GCT**GATCCAAGGCTGCCT	-3'
	Reverse	5'-	AGGCAGCCTTGGATC**AGC**TTTCACCATACCGTT	-3'
F425A	Forward	5'-	GATCCAAGGCTGCCT**GCT**GGTGGTACCAAACGC	-3'
	Reverse	5'-	GCGTTTGGTACCACC**AGC**AGGCAGCCTTGGATC	-3'
EcSSADH primer				
NdeI_F	Forward	5'-	GGAATTCATATGAAACTTAACGACAGTAAC	-3'
XhoI_R	Reverse	5'-	AACCGCTCGAGTTAAAGACCGATGCACATATATTT	-3'

Restriction sites used for cloning are underlined, and the boldfaced-underlines show the mutated sequences

2.5 Activity assays under H_2O_2-dependent oxidative stress

To characterize the functional role of the cofactor–cysteine adduct in response to oxidation, the dehydrogenase activity of SySSADH was measured under various levels of H_2O_2-dependent oxidative stress. To rule out the possible contribution of the reducing agent DTT in this assay, purification of SySSADH was carried out in the absence of DTT as described in the above section "2.4 Dehydrogenase activity assays" and its activity was measured using DTT-free standard assay solution, unless otherwise specified. EcSSADH (16, 17) was also purified in the absence of DTT as described above.

3. Results

3.1 Overall structure of apo-SySSADH

SySSADH is a dimeric protein in solution as characterized by size-exclusion chromatography (Figure 6). Consistent with this observation, no higher oligomerization states were evident from the crystallographic symmetry of the $P2_12_12_1$ space group. Therefore, the two monomers in an asymmetric unit represent the functional unit of the dimer and are related by a non-crystallographic twofold symmetry with a root mean-square deviation (RMSD) of 0.10 Å for 452 Cα atoms from Ile-3 to Lys-454.

The overall structure of monomeric SySSADH is reminiscent of an ALDH fold (28) and similar to the structures of HsSSADH (15) and EcSSADH (16, 17). It is made up of three segments: α/β-fold N- and C-domains for a cofactor-binding and a catalytic domain, respectively, and three antiparallel β-strands constituting a dimerization domain (Figures 3 and 7). Specifically, the N-domain (residues 3–103, 121–230, 420–444) contains a five-stranded parallel β-sheet (β5–β9) sandwiched between three helices (α1, α6, α7) on one side and four helices (α2, α3, α4, α5) on the other side. The seven-stranded parallel β-sheet (β10–β16) in the C-domain (residues 231–419) is flanked by three helices (α10–α12) and two helices (α8, α9). Juxtaposition of the N- and C-domains generates an active site tunnel between the two domains, which is accessible from both ends. The catalytic residues are located in the middle of the tunnel. A nucleophile Cys-262 is located in the catalytic loop between α8 and β11 of the C-domain, and a general base Glu-228 is located in an interdomain-connecting loop between β9 and β10. Due to these functional features, this structure is referred to as the active site tunnel. Dimerization is mediated

largely by N-domain α7 and the three antiparallel β-strands (β3, β4, β17) protruding from the N- and C-domains, resulting in a total of 2313 $Å^2$ for the buried surface area.

In addition to these structural features, which are also observed in other SSADHs, the binding sites of a phosphate ion and ethylene glycol near the entrance of the tunnel were identified (Figure 8). These sites act as a binding site for cofactor (see below). Specifically, the phosphate ion from the crystallization buffer is located at the N-terminus of α6 and the C-terminus of β6 in the N-domain. The hydroxyl group and the main chain nitrogen atom of Ser-157, and the side chain amino group of Lys-154, form possible hydrogen bonds within 3.0 Å of the oxygen atoms of the phosphate ion. In addition to these contacts, the positive helix dipole at the N-terminus of α6 likely stabilizes the binding of the phosphate ion.

Figure 6. **A size exclusion chromatography elution profile of SySSADH.** An elution profile from size-exclusion chromatography is shown for SySSADH (red) and a molecular marker (blue). The molecular weight of each marker is indicated by its elution peak.

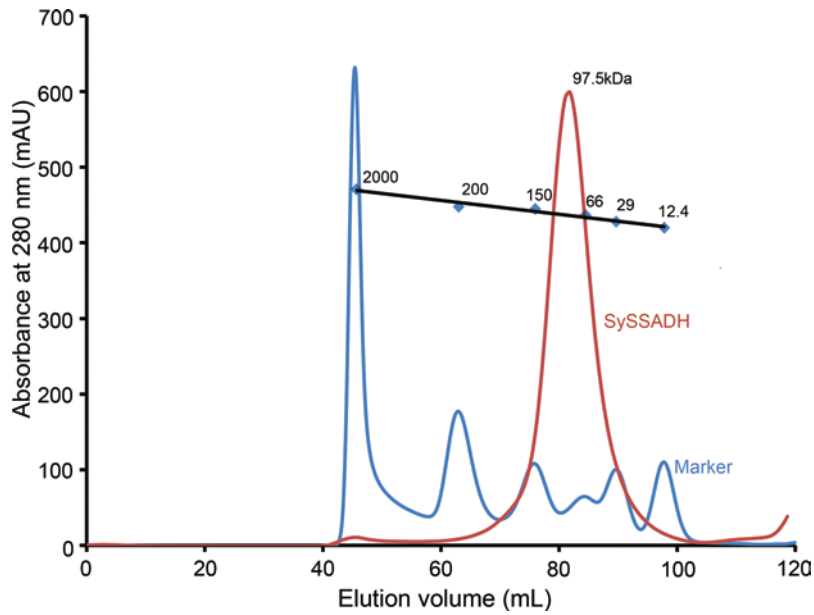
Absorbance at 280 nm (mAU)
Elution volume (mL)
97.5kDa
2000
200
150
66
29
12.4
SySSADH
Marker

Figure 7. **An overall structure of SySSADH.** The binary complex of SySSADH is shown with $NADP^+$, which is structurally similar to the apo form. Two monomers in an asymmetric unit are displayed. For clarity, $NADP^+$ is shown in only one of the monomers as a space-filling model. Monomeric SySSADH is composed of three domains: the cofactor-binding domain (pink), the catalytic domain (cyan), and the dimerization domain (green). Secondary structural elements are defined in Figure 3.

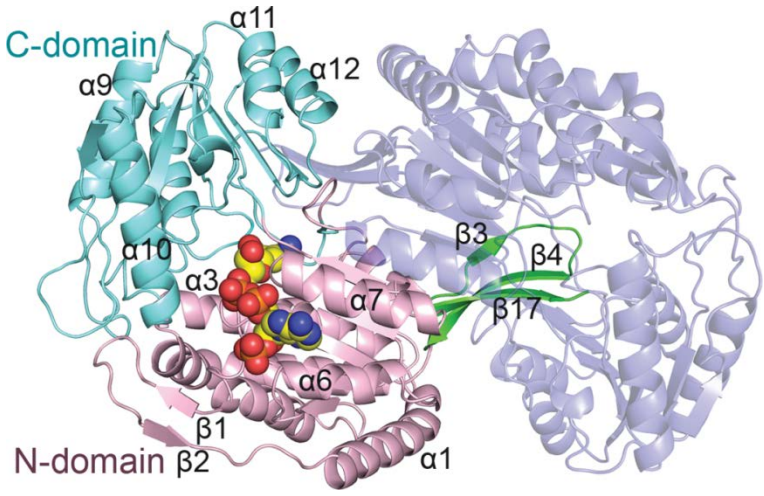
C-domain
α11
α12
α9
α10
α3
α7
β3
β4
β17
α6
β1
N-domain β2
α1

Figure 8. **The binding site for the phosphate ion and ethylene glycol in the apo structure of SySSADH.** The binding site of the phosphate ion and ethylene glycol in the apo structure of SySSADH is displayed in a stereo diagram. Those molecules are overlaid with $2F_o - F_c$ electron density maps (1.0 σ), and residues interacting with phosphate ion and ethylene glycol are indicated in yellow and cyan, respectively. Each subunit contained a total of 15 molecules of ethylene glycol, which was used as a cryoprotectant. Three molecules of ethylene glycol are localized at the entrance of the active site tunnel, and their positions are stabilized by Glu208, Gly230, Asp312, Gln316, Glu359, and Phe361.

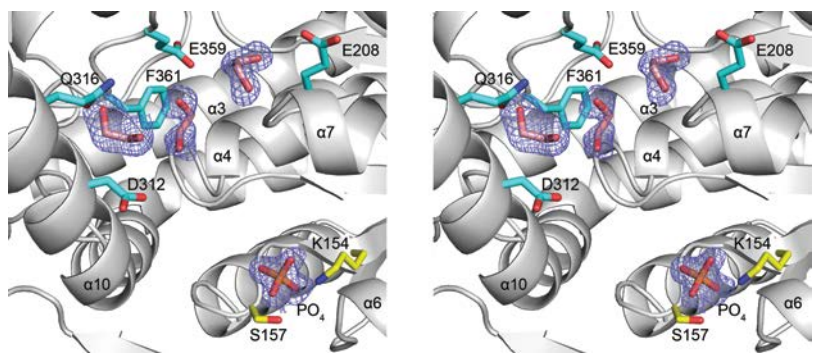
E359
E208
Q316
F361
α3
α7
α4
D312
K154
α10
PO4
α6
S157
E359
E208
Q316
F361
α3
α7
α4
D312
K154
α10
PO4
α6
S157

3.2 Structure of SySSADH in a binary complex with $NADP^+$

Structural analysis of the binary complex revealed a covalent linkage between the catalytic residue Cys-262 and the C4 atom on the nicotinamide ring of a cofactor (Figures 9 *A*-*E*). Formation of this adduct occurred when $NADP^+$, not NADPH, was present. This was true even when a crystal of SySSADH was soaked with NADPH. NADPH was later discovered to be spontaneously oxidized to $NADP^+$ under these experimental conditions (Figure 10).

One molecule of the cofactor adduct with Cys-262 was clearly located in each subunit (Figures 9 *A*-*C*). Overall, the cofactor moiety in the adduct adopted an extended conformation, with the nicotinamide ring and its associated ribose being completely buried in the tunnel (Figure 9*D*). The newly formed covalent linkage to the sulfur atom of Cys-262 was mediated with a *pro*-R face at C4 of the nicotinamide ring (Figure 9*E*), resulting in an sp^3 configuration at C4 of the nicotinamide ring, with bond angles of 108° and 109° for the C3–C4–S and C5–C4–S linkages, respectively (Figure 9*B*). The carbonyl amide group of the ring interacts with the side chains of Arg-139 and Glu-228 within 3.3 Å (Figure 9*E*). The position of ribose is stabilized by hydrogen bonds of 2.8 Å between Glu-359 and the 2'- and 3'-hydroxyl groups, and by possible hydrophobic interactions with Phe-361. The pyrophosphate group of the cofactor maintains only a few contacts with residues near the active site tunnel, forming hydrogen bonds with several water molecules and with the side chain nitrogen atom of Trp-130 and the hydroxyl group of Ser-207. In contrast, a ribose in the adenosine moiety is located near the entrance of the tunnel at a site enclosed by α6 and α7 in the N-domain. Specifically, the 2'-phosphate group in the ribose moiety occupies the binding site of the

phosphate ion that was identified in the apo form. Almost identical binding modes were observed with Ser-157 and Lys-154. The 3'-hydroxyl group mediates a possible hydrogen bond to the main chain carbonyl oxygen atoms of Met-128 and His-155. The adenine base is inserted into a concave, hydrophobic pocket formed between the α6 and α7 helices with its aromatic ring parallel to the helical axes of those two helices and surrounded by Ala-187 and Val-190 in α6 and Ala-210 and Leu-214 in α7. An additional binding site for ethylene glycol was also identified in the binary complex (Figure 11). It is located in the active site tunnel opposite the cofactor entrance and is located approximately 4.0 Å from Cys-262.

Figure 9. **The cofactor–cysteine adduct and its binding mode in the binary complex.** *A*, The NADP–cysteine adduct is shown with $NADP^+$ (yellow) and Cys-262 (green). The illustration is overlaid with an omitted $2F_o - F_c$ electron density map contoured at 1.0 σ. *B*, A different view of the NADP–cysteine adduct is shown, with an omitted $2F_o - F_c$ electron density map (1 σ). Atoms in the nicotinamide ring are labeled. During refinement, the distance between the C4 atom of the nicotinamide ring and the sulfur atom of Cys-262 was restricted to 1.9 Å, based on values predicted by quantum mechanical calculations (29) and an observed $F_o - F_c$ electron density map. *C*, The binary complex was refined in the absence of a covalent linkage between the cofactor and Cys262. The resulting model for the nicotinamide ring was then deviated from a $2F_o - F_c$ electron density map (1 σ), validating the presence of a covalent bond between the cofactor and Cys262. *D*, The binding mode of the cofactor–cysteine adduct is shown in an orientation identical with that of Figure 9*A*. The model for the adduct is represented in a ball-and-stick model. The nicotinamide moiety is buried in the active site tunnel while pyrophosphate and the adenosine moiety are bound to the positively charged region of SySSADH. *E*, The NADP moiety in the adduct is represented in a stereo view with its binding environment. Residues interacting with $NADP^+$ are included, along with water molecules (red sphere). See text for details of the interactions.

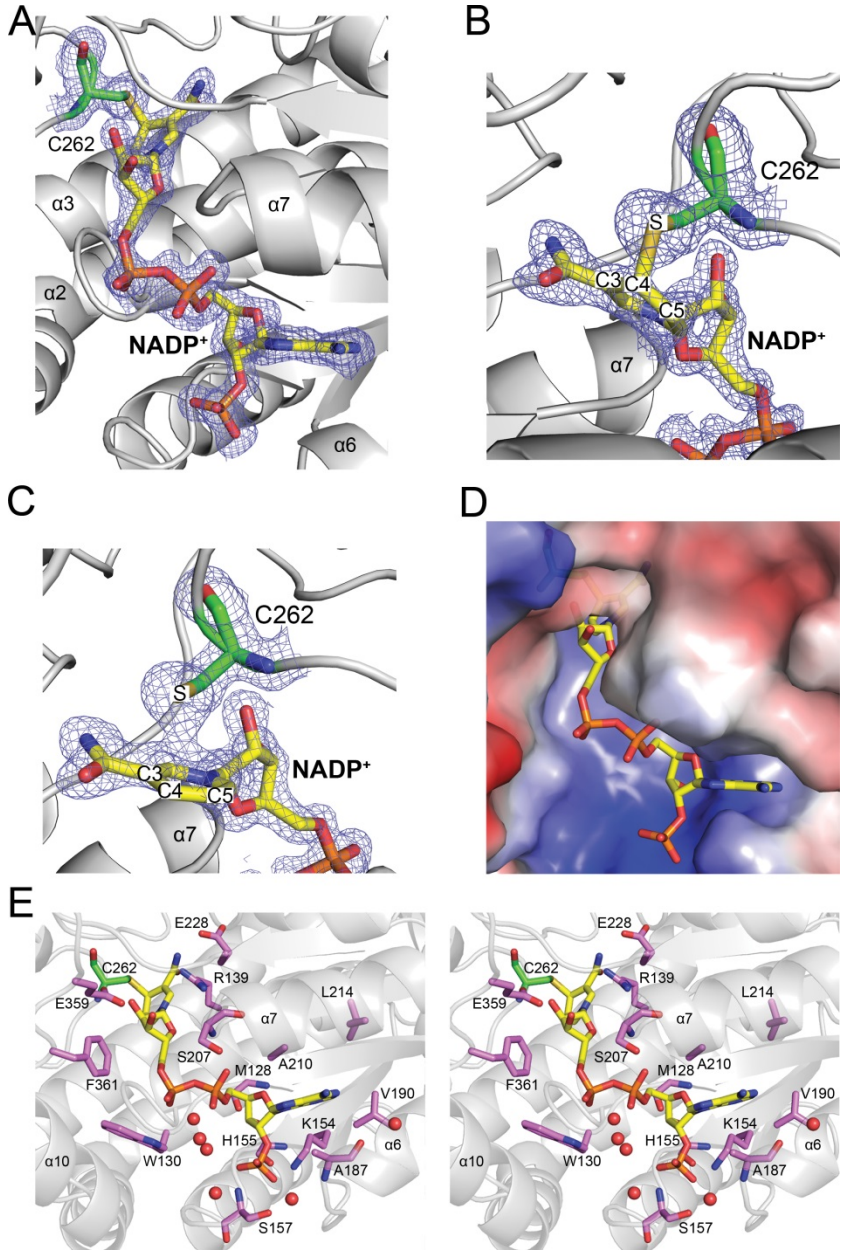
A
C262
α3
α7
α2
NADP+
α6
B
C262
S
C3
C4
C5
NADP+
α7
C
C262
S
C3
C4
C5
NADP+
α7
D
E
E228
C262
R139
L214
E359
α7
S207
M128
A210
F361
V190
K154
H155
α6
α10
W130
A187
S157
E228
C262
R139
L214
E359
α7
S207
M128
A210
F361
V190
K154
H155
α6
α10
W130
A187
S157

Figure 10. **The oxidation of NADPH in soaking buffer condition.** The oxidation of NADPH into $NADP^+$ occurs during crystal soaking. The spectrum of 270 μM NADPH, which was dissolved in the crystal soaking solution, was recorded at 0 min (blue) and 160 min (red), showing a significant reduction in absorbance at 340 nm. This decrease was due to the formation of $NADP^+$, which was further validated by an observed increase in absorbance at 340 nm in response to the addition of SySSADH and SSA. For this reaction, the assay solution was added after 160 min and the final concentration was 100 mM HEPES (pH 7.6), 10 mM $CaCl_2$, 10 mM DTT, and 200 μM SSA. An excess of SySSADH (1.9 mg) was included mainly because SySSADH is readily precipitated in the crystal-soaking solution. After incubating for 2 min, the reaction mixture was centrifuged and the spectrum of the supernatant was recorded (green). In contrast, the spectrum of NADPH at an equivalent concentration remained constant even after 120 min (purple) in the standard assay solution.

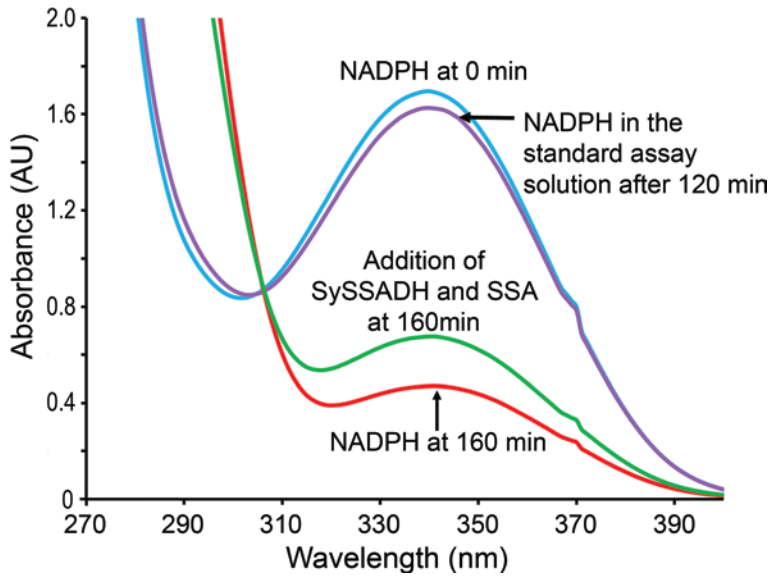
2.0
1.6
1.2
0.8
0.4
0
Absorbance (AU)
270
290
310
330
350
370
390
Wavelength (nm)
NADPH at 0 min
NADPH in the
standard assay
solution after 120 min
Addition of
SySSADH and SSA
at 160min
NADPH at 160 min

Figure 11. **An ethylene glycol molecule near the active site tunnel.** Ethylene glycol with a *2Fo – Fc* electron density map (1σ) is bound in the active site tunnel of the binary complex. It apparently came from the opening of the tunnel opposite the cofactor entrance and was located at about 4.0 Å from Cys262, with a hydrogen bonding distance of 3.8 Å to Lys86, Gln136, Arg139, and Ser419.

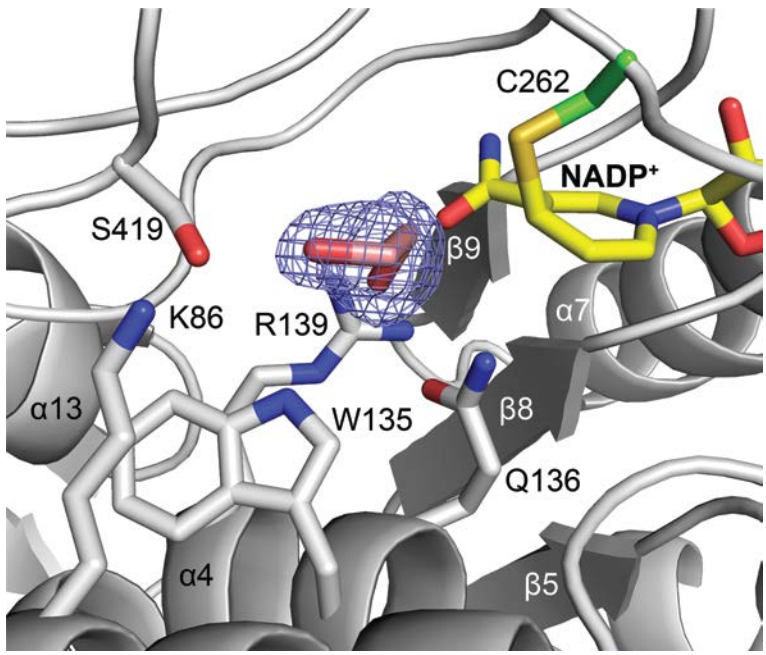
C262
NADP+
S419
β9
K86
R139
α7
α13
W135
β8
Q136
α4
β5

3.3 Ternary complex of SySSADH with NADPH and SSA

The presence of NADPH and SSA facilitated the formation of a ternary complex among SySSADH, the cofactor, and the substrate. Unlike in the binary complex, the cofactor remains as free NADPH, based on the sp^3 configuration of the C4 atom in the nicotinamide ring (Figures 12 *A* and *B*). SSA forms a covalent linkage with the catalytic residue Cys-262 (Figure 12*C*), resulting in a tetrahedral, thiohemiacetal intermediate (Figure 4).

NADPH in the ternary complex exhibits a bent conformation, with a large change in the dihedral angle of the pyrophosphate group. The nicotinamide moiety and its associated ribose is no longer in the active site tunnel but has moved away from the active site Cys-262 by about 5 Å toward the entrance of the tunnel, relative to its position in the binary complex. The nicotinamide ring, which is nearly at the position occupied by ribose in the binary complex, is further stabilized by possible stacking interactions with Phe-361. The carbonyl amide group of the nicotinamide ring interacts with nearby residues, including the side chains of Asn-131, Gln-136, Glu-228, as well as the main chain carbonyl oxygen atoms of Glu-228 and Leu-229. Several interactions are associated with ribose in the nicotinamide moiety and pyrophosphate group. Glu-359 maintains its interaction with the 2'-hydroxyl group of ribose, and water-mediated hydrogen bonds are predominant with the pyrophosphate group. Moreover, the 2'- and 3'-hydroxyl groups of ribose replace the binding site of ethylene glycol that was conserved in both the apo form and the binary complex. Except for these alterations, the binding environment for the adenosine moiety is essentially identical with that of the binary complex.

In the active site, the substrate SSA replaced the ethylene glycol that was identified in the binary complex. The bound SSA forms a covalent adduct with Cys-262 with angles of 109°, 119°, and 105° for the O–C4–S, O–C4–C3, and S–C4–C3 bonds, respectively (Figures 12 *C* and *D*). The SSA–cysteine adduct thus represents a thiohemiacetal intermediate in catalysis. The *re*-face of the trigonal C4 atom in SSA was subject to a nucleophilic attack by Cys-262 to produce an (*R*)-thiohemiacetal intermediate. The possible negative charge of the O4 atom in the intermediate can be neutralized by a hydrogen bond within 3.1 Å of the carbonyl amide group of NADPH and the side chain of Asn-131. The carboxyl group of SSA is within 3.0 Å of Trp-135, Arg-139, Ser-419, and several water molecules (Figure 12*D*). In addition to these hydrophilic residues, the binding site is enclosed by hydrophobic residues including Phe-132, Ile-263, and Phe-425.

Figure 12. **The binding mode of NADPH and SSA in a ternary complex with SySSADH.** *A*, The location of NADPH is shown with an omitted $2F_o - F_c$ electron density map contoured at 1.0 σ. Residues interacting with the nicotinamide group of NADPH are indicated. Note that the adenosine moiety resides in an almost identical binding environment in the binary and ternary complexes. The catalytic Cys-262 (green) and SSA (cyan) are also shown. *B*, The ternary complex contains an NADPH molecule, as displayed in the $2F_o - F_c$ electron density map contoured at 1.0 σ. Puckering of the nicotinamide ring in the cofactor indicates the presence of NADPH. *C*, The SSA–cysteine adduct is displayed in this orientation with an omitted $2F_o - F_c$ electron density map contoured at 1.0 σ. The modeled SSA (cyan) forms a thiohemiacetal intermediate with Cys-262 in the active site tunnel of SySSADH. Those residues exhibiting hydrophobic interactions and hydrogen bonds with SSA are presented. *D*, A schematic representation of the interactions in *C* is shown with an interatomic distance given in Å for possible hydrogen bonds. NADPH (yellow) and water molecules (red sphere) are also presented.

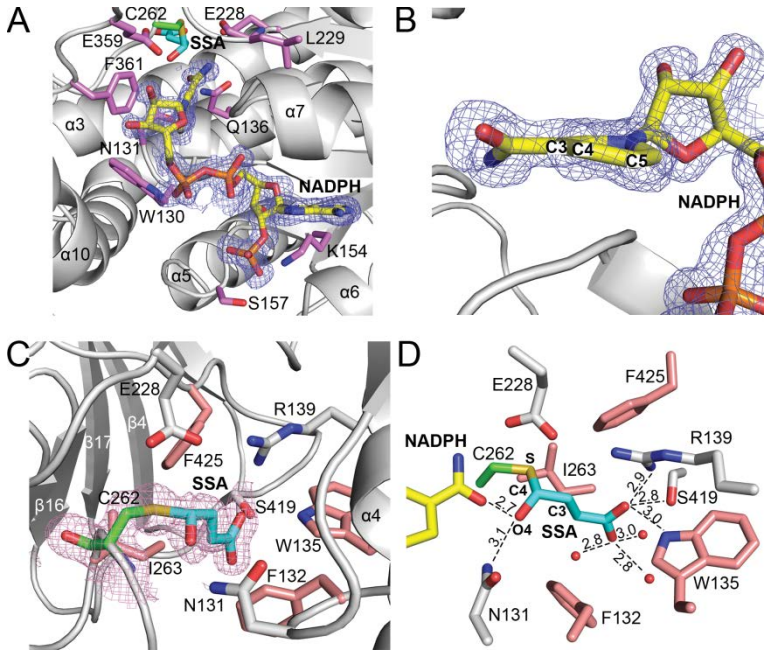
A
C262
E228
E359
SSA
L229
F361
α3
Q136
α7
N131
NADPH
W130
α10
K154
α5
S157
α6
B
C3
C4
C5
NADPH
C
E228
β4
R139
β17
F425
SSA
β16
C262
S419
α4
W135
I263
F132
N131
D
E228
F425
NADPH
C262
S
I263
R139
C4
S419
C3
O4
SSA
W135
N131
F132

3.4 Structural comparison of different ligation states

No significant changes were noted (within a RMSD of 0.10 Å for 452 Cα atoms) in the overall conformations of the three structures characterized in this study. Noticeable alterations occurring along the catalytic reaction were localized within the cofactor and active site residues. Specifically, different binding modes were observed for the cofactor in the binary and ternary complexes. These were associated with a 5 Å positional shift of the nicotinamide moiety along the tunnel and a change of 85° in the dihedral angle of C4–C5–O–P_N (Figures 13 *A*-*C*).

The catalytic loop (Asn-257 to Lys-266), which contains the nucleophile Cys-262, remains in the same position in each of the three ligation states. However, significant changes were observed in the position of the side chain of Glu-228. In the apo form, the side chain of Glu-228 is aligned along the wall of the tunnel (Figure 13*A*). While its orientation remains in this position in the binary complex, an intrusion of the cofactor into the tunnel results in interactions between Glu-228 and the carbonyl amide group of the nicotinamide ring (Figure 13*B*). The orientation of Glu-228 in the ternary complex differs from those in the apo form and binary complex and is now in the active site tunnel only 3.3 Å from the C4 atom of the thiohemiacetal intermediate, maintaining its interaction with NADPH (Figure 13*C*). The side chain of Arg-139 takes on a small-scale change from an interaction with the carbonyl amide group of the nicotinamide ring in the binary complex to an interaction with the carboxyl group of SSA in the ternary complex.

Figure 13. **Structural features of the active site residues in different ligation states.** Active site residues including Cys-262, Glu-228, Arg-139, and the catalytic loop (Asn-257 to Lys-266, magenta), are shown for; *A*, the apo form, *B*, the binary complex, and *C*, the ternary complex. $NADP^+$ (green) is included in *B*, and NADPH (yellow) and SSA (cyan) are indicated in *C*.

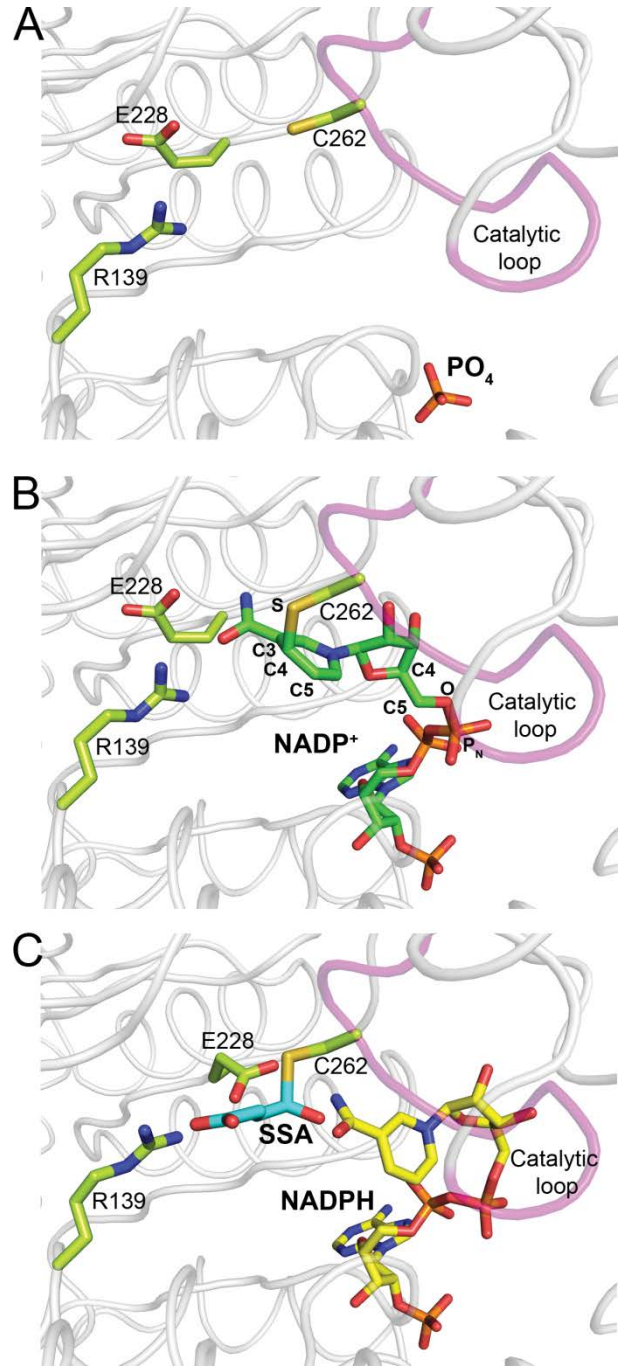
A
E228
C262
Catalytic loop
R139
PO4
B
E228
S
C262
C3
C4
C5
C4
O
C5
Catalytic loop
R139
NADP+
PN
C
E228
C262
SSA
Catalytic loop
R139
NADPH

3.5 Functional analysis of the active site residues

Preliminary experiments revealed several unusual aspects in the steady-state kinetics of SySSADH (Figures 14 *A*-*F*). In addition to the divalent metal- and DTT-dependent reaction activation, the most unexpected observations were large deviations in the initial velocity that were dependent on the order of the addition of substrate into the assay solution (Figure 14*A*). The SySSADH enzyme preincubated with $NADP^+$ showed a linear increase in absorbance after the addition of substrate SSA. Unless, the reaction progress profile exhibited a significant lag, rendering it impractical to reliably measure the initial velocity. Therefore, a standard assay solution was prepared containing DTT, $CaCl_2$, and the SySSADH enzyme. The reaction was initiated by adding 200 μM SSA (see below) after 10 min incubation with $NADP^+$. A K_m of 439 μM and V_{max} of 46 μM min^{-1} for $NADP^+$ were successfully measured with 200 μM SSA using the standard assay (Figure 14*E*). Those kinetic parameters were not reliably determined for SSA, mainly due to a non-hyperbolic change in initial velocity as a function of the SSA concentration (Figure 14*F*). However, the K_m of SSA was estimated to be far less than 50 μM. The catalytic activities of the WT and various mutant enzymes were measured using 200 μM SSA and 2.5 mM $NADP^+$.

The functional roles of various residues in the active site were evaluated (Figures 12*D* and 15). Consistent with the proposed catalytic role of Cys-262 as a nucleophile and Glu-228 as a general base, mutant enzymes such as C262A, E228A, and E228Q were essentially nonfunctional. The substrate SSA-binding region is also crucial for enzyme activity. Mutation of residues that interact with the O4 atom or the carboxyl group of SSA abolished enzyme activity, as observed

with mutants N131A, N131D, and S419A. The F425A mutant was also inactive, suggesting that Phe-425 plays an important role in substrate binding. Some mutants, including F132A, W135A, R139A, and I263A, exhibited an activity of about 10–30% that of the WT enzyme, indicating a contribution of these SSA-binding residues to the overall enzyme activity. The R139K mutant enzyme exhibited an activity up to 80% that of the WT enzyme, further suggesting the significance of a positively charged residue in the binding of the carboxyl group of SSA.

Figure 14. **Kinetic profiles of SySSADH.** The reaction rate profiles of SySSADH depend on various effects. All assays were carried out according to the standard assay protocol and using the standard assay solution unless otherwise specified. *A,* The order of addition with regard to the substrate is essential for linearization of the initial velocity. The third substrate is labeled. *B,* DTT (10 mM) and a divalent metal (10 mM) increased the initial velocity. The assay followed the standard protocol with various combinations of DTT and/or a divalent metal. *C,* A 10-min incubation of SySSADH and $NADP^+$ was enough to reach a maximum initial velocity. The incubation time of SySSADH and $NADP^+$ are indicated. Plots of the initial velocity as a function of substrate concentration are shown for; *D*, $CaCl_2$, *E*, $NADP^+$, and *F*, SSA.

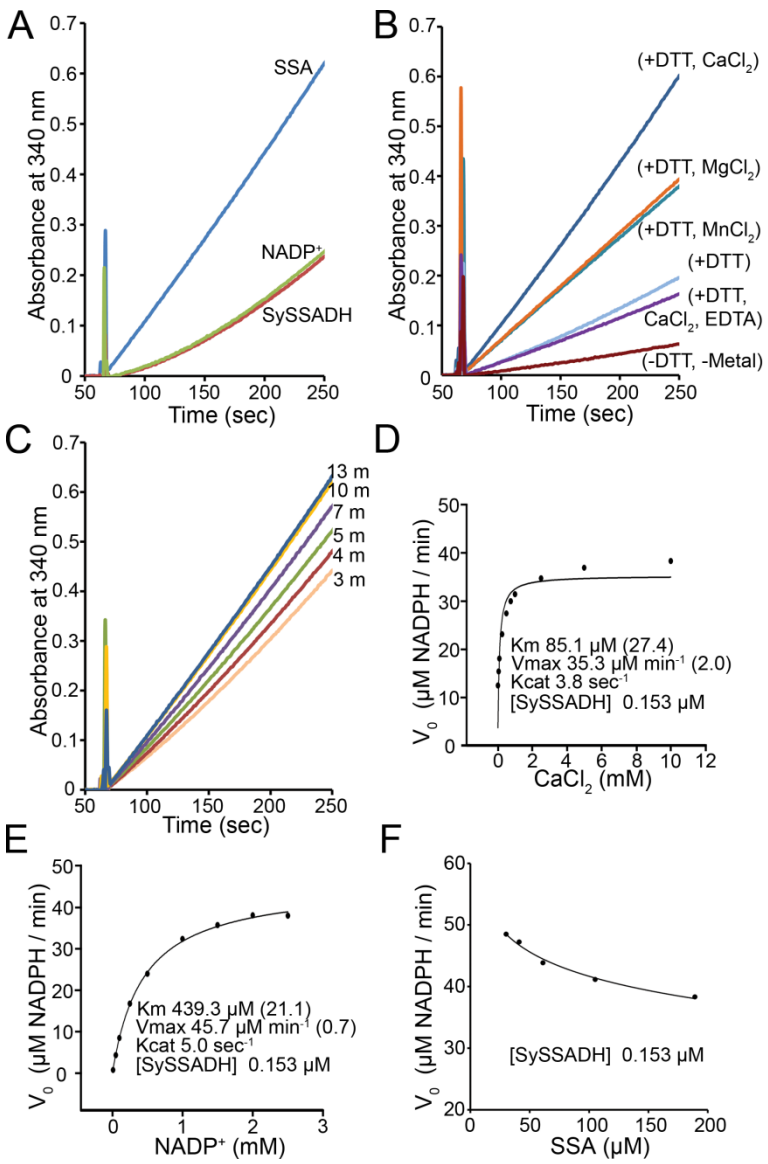
A
Absorbance at 340 nm
Time (sec)
SSA
NADP+
SySSADH
B
Absorbance at 340 nm
Time (sec)
(+DTT, CaCl2)
(+DTT, MgCl2)
(+DTT, MnCl2)
(+DTT)
(+DTT, CaCl2, EDTA)
(-DTT, -Metal)
C
Absorbance at 340 nm
Time (sec)
13 m
10 m
7 m
5 m
4 m
3 m
D
V0 (µM NADPH / min)
CaCl2 (mM)
Km 85.1 µM (27.4)
Vmax 35.3 µM min-1 (2.0)
Kcat 3.8 sec-1
[SySSADH] 0.153 µM
E
V0 (µM NADPH / min)
NADP+ (mM)
Km 439.3 µM (21.1)
Vmax 45.7 µM min-1 (0.7)
Kcat 5.0 sec-1
[SySSADH] 0.153 µM
F
V0 (µM NADPH / min)
SSA (µM)
[SySSADH] 0.153 µM

Figure 15. **Functional analysis of the active site residues in SySSADH.** The initial velocity of various mutant enzymes was compared with that of the WT enzyme. See "Materials and Methods" for experimental details.

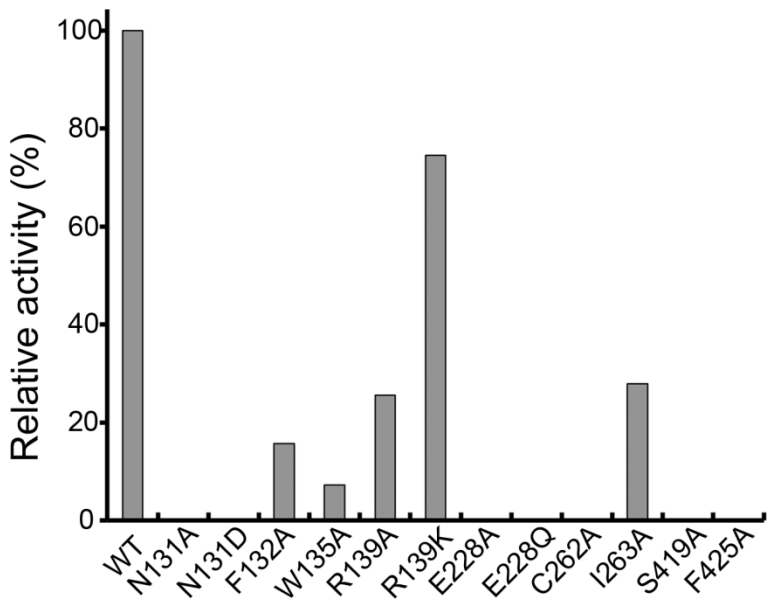
Relative activity (%)
100
80
60
40
20
0
WT
N131A
N131D
F132A
W135A
R139A
R139K
E228A
E228Q
C262A
I263A
S419A
F425A

3.6 Formation of an NADP-cysteine adduct in solution

To validate the presence of a cofactor–cysteine adduct in solution, spectrophotometric measurements were performed in which an equimolar (16 μM) solution of SySSADH and $NADP^+$ was incubated in a standard assay solution. Absorbance was measured from 300 to 400 nm, which corresponds to the absorbance of the proposed adduct (21, 30). Such an absorption occurred only in the co-presence of SySSADH and $NADP^+$ (Figure 16*A*) and disappeared when the WT enzyme was replaced with the C262A mutant (Figure 16*B*), thereby validating the formation of an adduct with Cys-262.

Figure 16. **The formation of the cofactor–cysteine adduct in solution using the WT enzyme and the C262A mutant.** Spectra were recorded for 16 μM SySSADH (red), 16 μM $NADP^+$ (blue), and a mixture of 16 μM SySSADH and $NADP^+$ (green). Specifically, each sample was incubated for 120 min in an assay solution of 100 mM HEPES (pH 7.6), 10 mM $CaCl_2$, and 10 mM DTT. A possible adduct occurs using; *A*, the WT enzyme but does not take place with *B*, the C262A mutant enzyme.

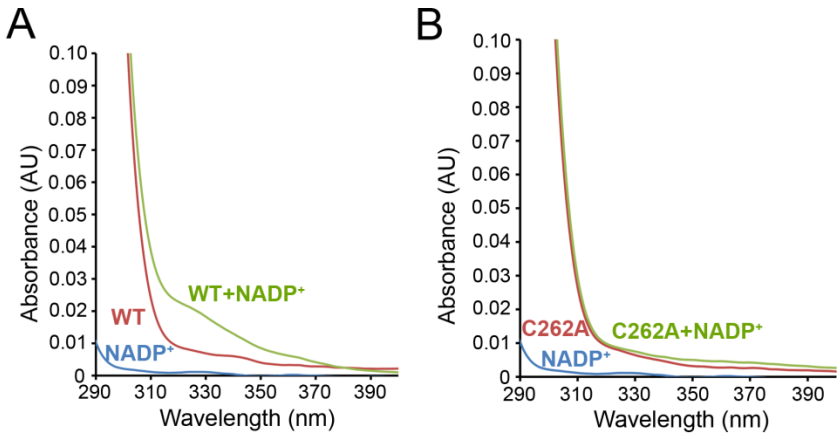
A
Absorbance (AU)
0.10
0.09
0.08
0.07
0.06
0.05
0.04
0.03
0.02
0.01
0
290
310
330
350
370
390
Wavelength (nm)
WT+NADP+
WT
NADP+
B
Absorbance (AU)
0.10
0.09
0.08
0.07
0.06
0.05
0.04
0.03
0.02
0.01
0
290
310
330
350
370
390
Wavelength (nm)
C262A
C262A+NADP+
NADP+

3.7 Cofactor-dependent oxidation protection in SySSADH

Previous structural and functional analyses of 2-Cys HsSSADH showed that HsSSADH is inactivated by H_2O_2-dependent oxidative stress. Its activity is recovered by adding DTT, which suggests that a nucleophilic cysteine remains protected under oxidizing conditions via the formation of a disulfide bridge with the second cysteine in the catalytic loop, and that the reduced cysteine is required for activity (15). Due to the lack of a second cysteine, such a mechanism is unavailable in SySSADH, as well as in other members of the 1-Cys SSADH family. This leaves the question of whether SySSADH activity is affected by oxidation and how the nucleophilic cysteine of SySSADH can be protected in oxidizing conditions. Given the crystallographic and spectrophotometric identification of the cofactor–cysteine adduct, and the linearity of the initial velocity following preincubation with $NADP^+$, hypothesized that the formation of a cofactor–cysteine adduct is kinetically preferred and could play a role in oxidation protection of the catalytic cysteine.

Five independent assays for SySSADH activity were performed under H_2O_2-dependent oxidative stress with 50–1000 μM H_2O_2 and variations of DTT and $NADP^+$ (Figure 17). To rule out the possible contribution of a reducing agent DTT in this assay, SySSADH was purified in the absence of DTT and its resulting activity was also measured in a DTT-free standard assay solution, unless otherwise specified. The results were then compared with those obtained in the absence of H_2O_2. From the first set of experiments (the blue columns), SySSADH was found to be sensitive to H_2O_2-dependent oxidation. The enzyme activity at 50 μM H_2O_2 was sharply reduced to 31% of the H_2O_2-free enzyme and further decreased to 3%

at 1000 μM H_2O_2. Oxidation effects were nearly eliminated by the co-presence of 10 mM DTT at the onset of the reaction (the red columns), indicating that the reduction in activity of the first set is attributable to H_2O_2-dependent oxidation. The addition of DTT at 60 min after the H_2O_2 treatment (the green columns) was not able to fully recover the enzyme activity. However, more than 70% of the original SySSADH activity was maintained with 50–250 μM H_2O_2 with a further drop of activity to 40% at 1000 μM H_2O_2. Comparable or even higher enzyme activity was observed in the fourth set of experiments (the lavender columns) in which SySSADH was preincubated for 10 min with 2.5 mM $NADP^+$ followed by H_2O_2 treatment for 60 min. In particular, if SySSADH is preincubated in the presence of both $NADP^+$ and DTT, its activity is fully protected even after treatment with 1000 μM H_2O_2 (the magenta column). This suggests that under reducing conditions, the catalytic cysteine binds preferentially to a cofactor and remains in a fully active form. This analysis indicates that while SySSADH activity is subject to oxidation, the formation of a cofactor–cysteine adduct plays a key role in protecting the catalytic Cys-262 from oxidation. Furthermore, the adduct is readily dissociable in the presence of a SSA substrate.

Figure 17. **Redox-dependent activity regulation in SySSADH.** The catalytic activity of 1-Cys SySSADH was measured under H_2O_2-dependent oxidative stress in a range of 50–1000 μM H_2O_2. In all experiments, the initial velocity was measured at 70 min of reaction by adding 200 μM SSA (S in a table) after various pretreatments, including H_2O_2 (H), 2.5 mM $NADP^+$ (N), and/or 10 mM DTT (D). The resulting activities were compared with those of a control experiment in the absence of H_2O_2 (the black column at 0 μM H_2O_2). Five different experiment conditions are indicated by different colors.

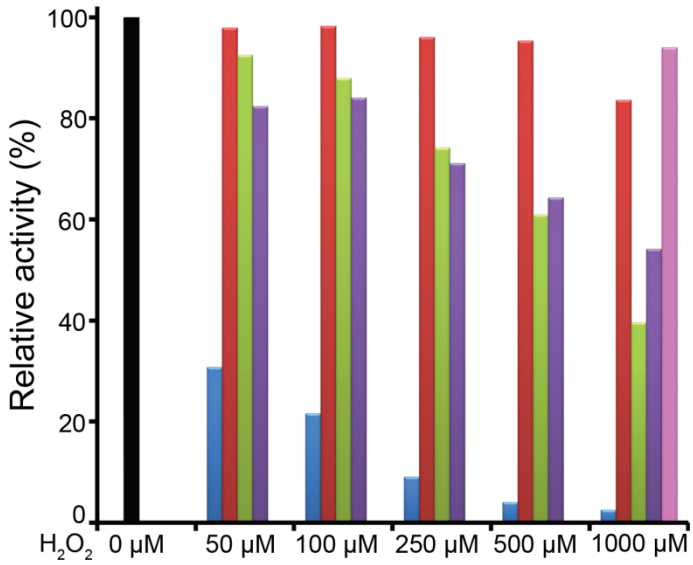

Rx time		0 min	10 min	60 min	70 min
First		H		N	S
Second		H+D		N	S
Third		H		N+D	S
Fourth		N	H		S
Fifth		N+D	H		S

3.8 Redox-dependent activity regulation in a 2-Cys EcSSADH

Previous functional studies of 2-Cys EcSSADH from two independent groups provided contradictory results regarding the presence of a redox-dependent regulatory mechanism in EcSSADH (16, 17). Therefore, the current study addresses whether redox-dependent regulation is present in a 2-Cys EcSSADH and how the enzyme responds to a cofactor. For this assay, EcSSADH was purified in the absence of DTT. First, using the standard assay solution containing 10 mM DTT, EcSSADH was found to require a preincubation with $NADP^+$ to yield a linear initial velocity and a catalytically competent reaction. This was the case unless the enzyme exhibited a lag phase with lower values of initial velocity (an insert in Figure 18), which suggests the formation of a cofactor–cysteine adduct in the reduced enzyme.

The activity of EcSSADH was measured under various oxidizing and reducing conditions (Figure 18). In Assay A, a residual activity (5.4 μM min^{-1}) was measured in the absence of DTT and H_2O_2 after 10-min incubation with $NADP^+$, suggesting that the purified enzyme contains some fraction of catalytically competent cysteine in its reduced form. Significant variations were observed under oxidizing conditions with 1000 μM H_2O_2, particularly in the presence of 10 mM DTT at 0, 60, or 70 min into the reaction. In the co-presence of H_2O_2 and DTT at 0 min (Assay B), an EcSSADH activity of 9.7 μM min^{-1} was measured, which is higher than a residual activity. However, the presence of DTT at 60 min in a solution with preexisting H_2O_2 (Assay C) showed a large increase in EcSSADH activity to 20.3 μM min^{-1}, while a marginal activity of 1.7 μM min^{-1} was observed with an addition of DTT at 70 min in Assay D. These large variations in activity are

readily explained if the catalytic cysteine remains in its oxidized form in the presence of H_2O_2, maintained by the formation of a disulfide bond with the second cysteine in the catalytic loop, as observed with 2-Cys HsSSADH (15). Under these conditions, the addition of DTT at 60 min (Assay C) reduces the disulfide bond, resulting in a catalytically competent cysteine. However, the functionally inactive, oxidized form of the catalytic cysteine remains dominant in Assay D. The presence of both reduced and oxidized cysteine in Assay B, due to the co-presence of DTT and H_2O_2, likely resulted in the enzyme activities between Assays C and D.

In contrast, under the reducing conditions presented by the co-presence of $NADP^+$ and DTT, enzyme activity increased significantly and the enzyme became resistant to oxidative stress. A maximal activity of 39.6 μM min^{-1} (Assay E) was observed after 10 min incubation. This is twofold higher than the activity observed following oxidation and subsequent reduction as in Assay C. Further treatment with H_2O_2 for 60 min under these conditions resulted in an enzyme activity of 30.9 μM min^{-1} (Assay F). However, differences in activity between Assays E and F are not due to H_2O_2-dependent oxidative stress, but by some uncharacterized effects caused by the 60-min incubation. A similar reduction of activity was observed in Assay G, in which H_2O_2 was not included in the assay solution but the reaction mixture was incubated for an additional 60 min. In principle, the activities in Assays C and E (20.3 μM min^{-1} and 39.6 μM min^{-1}, respectively) should be comparable since the catalytic cysteine remains in its functionally active form in both cases. The apparently lower activity of Assay C is likely due to the catalytically active cysteine being in its reduced form, which is responsible for the residual activity (5.4 μM min^{-1}) observed in Assay A. This leaves the cysteine

subject to oxidation in Assay C. A reduction of activity by as much as 13.8 μM min^{-1}, caused by an unspecified mechanism, was associated with the 60-min incubation time in Assay H. Considering a total reduction of 19.2 μM min^{-1}, the enzyme activities in Assay C and E are clearly equivalent.

These results strongly support the hypothesis that the catalytic cysteine in 2-Cys EcSSADH exists in an oxidized form as a disulfide bridge under oxidizing conditions. The disulfide bond is then fully switched into a catalytically active, reduced form under reducing conditions. Furthermore, once reduced, the catalytic cysteine preferentially forms an NADP–cysteine adduct if $NADP^+$ is present. The resulting adduct becomes resistant to H_2O_2-dependent oxidative stress. Therefore, 2-Cys EcSSADH appears to be equipped with two different levels of redox-dependent regulation: disulfide bond formation in the oxidized state and the formation of an NADP–cysteine adduct in the reduced state.

Figure 18. **Redox-dependent activity regulation in EcSSADH.** The catalytic activity of 2-Cys EcSSADH was measured under oxidizing conditions in 1000 μM H_2O_2 and/or under reducing conditions in 10 mM DTT. Initial velocities were measured as in Figure 15. except for Assays A and E, for which measurements were acquired after only 10 min. A reaction progress curve is shown in the insert where the third component indicated was added to the standard assay solution after a 10-min incubation of the other two components.

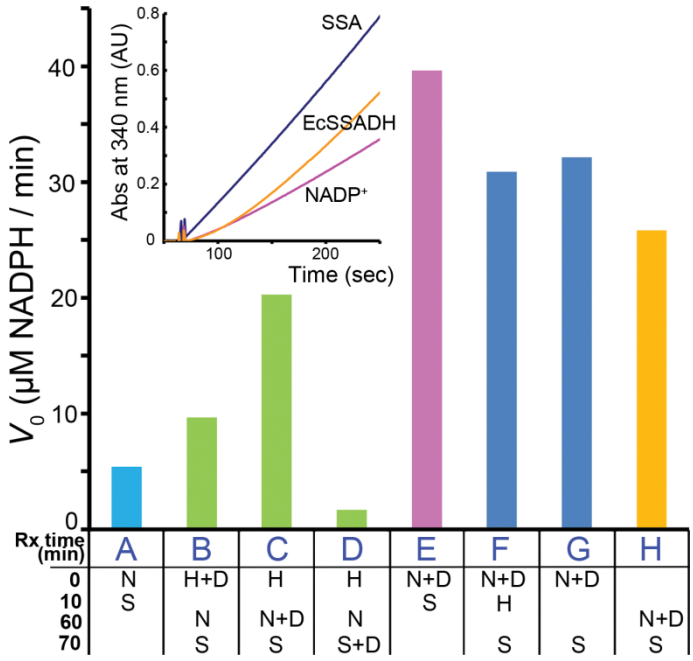
V_0 (μM NADPH / min)
0
10
20
30
40
Abs at 340 nm (AU)
0
0.2
0.4
0.6
0.8
100
200
Time (sec)
SSA
EcSSADH
NADP+
Rx time (min)
A
B
C
D
E
F
G
H
0
10
60
70
N
S
H+D
N
S
H
N+D
S
H
N
S+D
N+D
S
N+D
H
S
N+D
S
N+D
S
N+D
S

4. Discussion

From a structural perspective, SySSADH is highly homologous with members of the ALDH family (2). A DALI search (31) revealed that ALDH structures are similar to SySSADH with *Z*-scores of 14.3–58.6 and RMSDs of 1.1–4.4 Å for Cα atoms. However, these similarities were confined within the monomeric structure. Unlike the tetrameric structure exhibited by SSADHs from humans and *E. coli* (15-17), SySSADH is a dimeric protein, which is also characteristic of some members of the ALDH family (2). Extensive reports detailing the structural and functional features of the ALDH family are available (4, 32). Therefore, this section focuses on comparisons of SySSADH with other SSADHs.

From a functional perspective, SySSADH has two unique features relative to other SSADHs: an $NADP^+$-dependent activity and the presence of only one cysteine residue in the catalytic loop. Sequence conservations of the phosphate-binding sites and its accompanying structural features result in a preference for $NADP^+$ over NAD^+ in SySSADH (Figure 19*A*). In particular, structural and sequence comparisons have indicated that the residue equivalent to Ser-157 in SySSADH is likely a key determinant of cofactor specificity for NAD^+ or $NADP^+$.

The single cysteine residue, a nucleophilic Cys-262, in the catalytic loop represents another major difference from other 2-Cys SSADHs. This apparently minor variation exerts significant effects on enzyme properties including the static conformation for the catalytic loop, the binding mode of the cofactor, and oxidation protection. Note that most members of the ALDH family contain one cysteine in the catalytic loop and that only 68 of the 1000 members of the family have a catalytic loop with two cysteine residues (Figure 20). The catalytic loop (Asn-257

to Lys-266) in SySSADH adopts the same orientation throughout the reaction process (Figures 13 *A*-*C*), leaving the active site tunnel in an opened state. The SySSADH catalytic loop is essentially identical, within a RMSD of 0.3–0.4 Å for 10 Cα atoms, with that of HsSSADH in its reduced form (PDB code 2W8O) (15) and with that of reduced EcSSADH in its complex with $NADP^+$ (PDB code 3JZ4) (17). Since the nicotinamide moiety of the cofactor is bound in the tunnel, the conformation state of the active site tunnel affects the binding mode of the cofactor. In fact, the nicotinamide moiety in the SySSADH binary complex occupies the innermost position in the tunnel (Figures 9*A* and 19*B*). In the ternary complex, the nicotinamide moves back along the tunnel, mainly due to the binding of SSA to Cys-262 (Figure 13*C*). The resulting location of the cofactor is identical to that in reduced EcSSADH (17). These observations are similar to previous characterizations of the ALDH family in which the nicotinamide half of the cofactor exhibits two different binding mode conformations, "hydride transfer" and "hydrolysis" (33), as the reaction proceeds.

The identification of a covalent adduct between $NADP^+$ and Cys-262 in the binary complex of SySSADH is not an isolated example. Such an adduct was predicted by quantum mechanical calculations (29) and then characterized in two different structures from the ALDH family (21, 30, 34). However, to date, the functional role of the covalent adduct has remained elusive. The results of the current study suggest that the adduct serves to recruit a cofactor in the vicinity of the catalytic nucleophile for catalysis, particularly for hydride transfer. Perhaps more importantly, the adduct provides a novel means of protection against oxidative stress. SySSADH was shown to be an oxidation-sensitive enzyme

(Figure 17). Oxidation should occur at the nucleophile cysteine in the catalytic loop. Unlike 2-Cys HsSSADH, 1-Cys SySSADH lacks a second cysteine and is therefore unable to protect its highly reactive nucleophilic cysteine residue. Instead, SySSADH holds the catalytic loop static and adopts an open conformation with regard to the active site tunnel. Under these circumstances, the cofactor preferentially binds to and forms a covalent adduct with the thiolate of Cys-262. Once formed, the cofactor–cysteine adduct protects the catalytic cysteine from H_2O_2-dependent oxidative stress. More than 70% of SySSADH catalytic activity remains in the presence of as much as 250 μM H_2O_2 (Figure 17), despite the fact that oxidative stress *in vivo* occurs at much lower concentrations (35-37). This cofactor-dependent oxidation protection is likely applicable to other 1-Cys SSADHs. Moreover, the 1-Cys SSADH from *Mycobacterium tuberculosis* (Figure 3) also exhibited a pronounced lag phase when the enzyme was included as the final component in the reaction mixture (19), which suggests the presence of a cofactor–cysteine adduct. My analysis further suggests that 2-Cys EcSSADH has two different mechanisms for redox-dependent regulation. In particular, a cofactor–cysteine adduct is formed under reducing conditions (Figure 18). Taken together, the formation of a cofactor–cysteine adduct as a means of protecting the catalytic cysteine from possible oxidation is most likely common in members of the SSADH family and ALDH superfamily (21, 30). This unique mechanism differs from the redox regulation of tyrosine phosphatise 1B, when the thiolate of the catalytic cysteine forms a covalent bond with the main chain nitrogen of a nearby residue (38).

In this study, the crystal structures of an $NADP^+$-dependent SySSADH were determined that is involved in the TCA cycle in cyanobacterial *Synechococcus* sp. PCC 7002. The apo structure, as well as a binary complex with $NADP^+$ and a ternary complex with NADPH and SSA, revealed a structural basis for the formation of a cofactor–cysteine adduct and a thiohemiacetal intermediate, thereby providing details about the catalytic mechanism. In particular, the mechanistic details of SySSADH are similar to those in Figure 21 and the recently updated mechanism of the ALDH family (30). The current study provides additional insights including the preferred binding of $NADP^+$ over SSA, the nucleophilic attack of Cys-262 on the *re*-face of a trigonal C4 atom in SSA, and the formation of an (*R*)-thiohemiacetal intermediate. Further kinetic and functional analyses elucidated the functional properties of active site residues and revealed the preferential binding of $NADP^+$ to the catalytic cysteine. The formation of a cofactor–cysteine adduct was hypothesized to be a novel means of protecting the catalytic cysteine from oxidation and could be applicable to other members of the SSADH family.

Figure 19. **A structural comparison for the 2'-phosphate binding region and the relative position of cofactor in SySSADH.** *A*, The binding region is shown for the 2'-phosphate in ribose of the adenosine moiety in the cofactor: SySSADH (yellow), EcSSADH (green), and HsSSADH (cyan). HsSSADH utilizes NAD^+ as a cofactor while $NADP^+$ serves as the cofactor for SySSADH and EcSSADH. *B*, The structure superposition of $NADP^+$ in EcSSADH (green), $NADP^+$ in the SySSADH binary complex (yellow), and NADPH in the SySSADH ternary complex (magenta) is shown. The catalytic cysteine residue is indicated. The position of $NADP^+$ in EcSSADH is almost identical to that of NADPH in the SySSADH ternary complex while the cofactor in the SySSADH binary complex is in an innermost location.

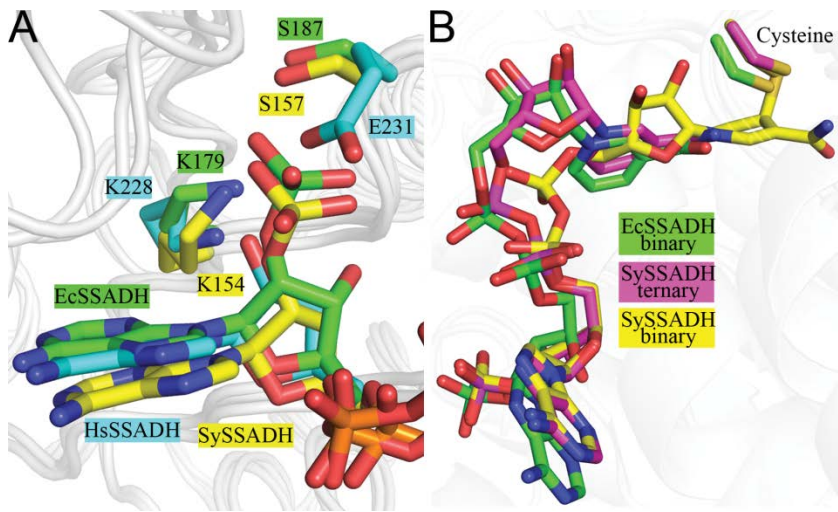
A
S187
S157
E231
K179
K228
K154
EcSSADH
HsSSADH
SySSADH
B
Cysteine
EcSSADH binary
SySSADH ternary
SySSADH binary

Figure 20**. The sequence alignment of SySSADH with members of the 2-Cys ALDH family.** The amino acid sequences of 2-Cys SSADHs were aligned with that of 1-Cys SySSADH. A BLAST search indicated that 68 of 1000 putative SSADHs are 2-Cys SSADHs. The general base glutamate and catalytic cysteine are indicated on a red background while the second cysteine is on a green background. Highly conserved residues are shown on a gray background.

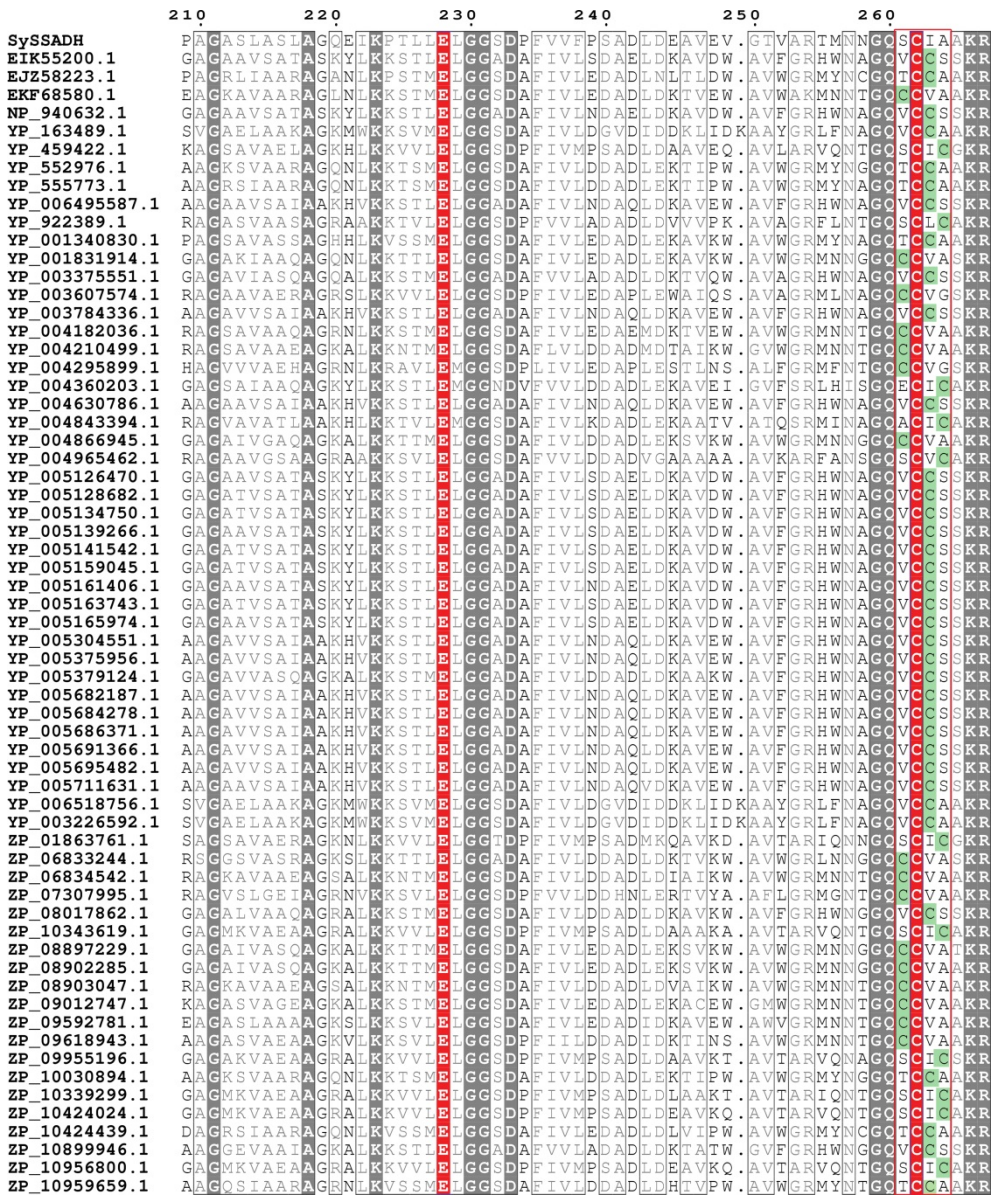
210
220
230
240
250
260
SySSADH
EIK55200.1
EJZ58223.1
EKF68580.1
NP_940632.1
YP_163489.1
YP_459422.1
YP_552976.1
YP_555773.1
YP_006495587.1
YP_922389.1
YP_001340830.1
YP_001831914.1
YP_003375551.1
YP_003607574.1
YP_003784336.1
YP_004182036.1
YP_004210499.1
YP_004295899.1
YP_004360203.1
YP_004630786.1
YP_004843394.1
YP_004866945.1
YP_004965462.1
YP_005126470.1
YP_005128682.1
YP_005134750.1
YP_005139266.1
YP_005141542.1
YP_005159045.1
YP_005161406.1
YP_005163743.1
YP_005165974.1
YP_005304551.1
YP_005375956.1
YP_005379124.1
YP_005682187.1
YP_005684278.1
YP_005686371.1
YP_005691366.1
YP_005695482.1
YP_005711631.1
YP_006518756.1
YP_003226592.1
ZP_01863761.1
ZP_06833244.1
ZP_06834542.1
ZP_07307995.1
ZP_08017862.1
ZP_10343619.1
ZP_08897229.1
ZP_08902285.1
ZP_08903047.1
ZP_09012747.1
ZP_09592781.1
ZP_09618943.1
ZP_09955196.1
ZP_10030894.1
ZP_10339299.1
ZP_10424024.1
ZP_10424439.1
ZP_10899946.1
ZP_10956800.1
ZP_10959659.1

Figure 21. **A proposed reaction mechanism for SySSADH.**

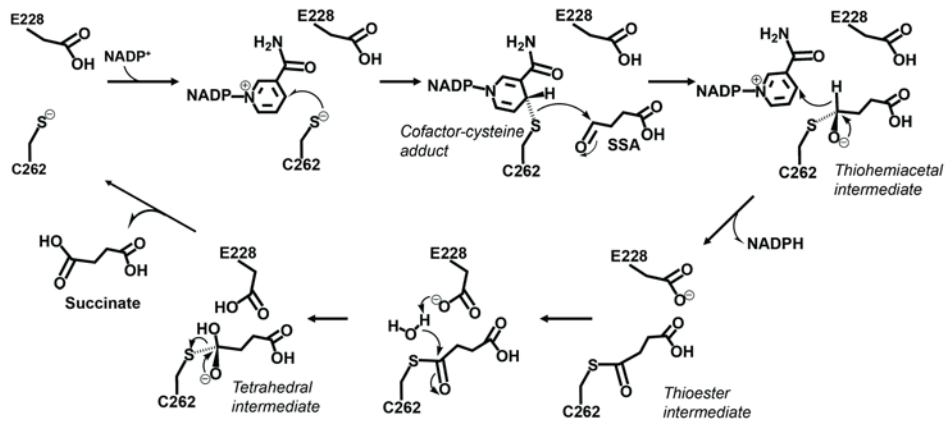
E228
NADP+
NADP
C262
Cofactor-cysteine adduct
SSA
Thiohemiacetal intermediate
NADPH
Thioester intermediate
Tetrahedral intermediate
Succinate

5. References

1. Kirch, H., Bartels, D., Wei, Y., Schnable, P. S., and Wood, A. J. (2004) The ALDH gene superfamily of *Arabidopsis*. *Trends Plant Sci.* 9, 371-377
2. Perozich, J., Nicholas, H., Wang, B. C., Lindahl, R., and Hempel, J. (1999) Relationships within the aldehyde dehydrogenase extended family. *Protein Sci.* **8**, 137-146
3. Zakhari S. (2006) Overview: how is alcohol metabolized by the body? *Alcohol Res. Health.* **29**,245-254.
4. Muñoz-Clares, R. A., González-Segura, L., and Díaz-Sánchez, A. G. (2011) Crystallographic evidence for active-site dynamics in the hydrolytic aldehyde dehydrogenases. Implications for the deacylation step of the catalyzed reaction. *Chem. Biol. Interact.* **191**, 137-146
5. Watanabe, M., Maemura, K., Kanbara, K., Tamayama, T., and Hayasaki, H. (2002) GABA and GABA receptors in the central nervous system and other organs. *Int Rev Cytol.* **213**, 1-47.
6. Fait, A., Fromm, H., Walter, D., Galili, G., and Fernie, A. R. (2008) Highway or byway: the metabolic role of the GABA shunt in plants. *Trends Plant Sci.* **13**, 14-19
7. Kim, K., Pearl, P. L., Jensen, K., Snead, O. C., Malaspina, P., Jakobs, C., and Gibson, K. M. (2011) Succinic semialdehyde dehydrogenase: Biochemical–molecular–clinical disease mechanisms, redox regulation, and functional significance. *Antioxid. Redox Signal* **15**, 691-718

8. Pearl, P. L., Novotny, E. J., Acosta, M. T., Jakobs, C., and Gibson, K. M. (2003) Succinic semialdehyde dehydrogenase deficiency in children and adults. *Ann. Neurol.* **54**, S73-80.
9. Malaspina, P., Picklo, M. J., Jakobs, C., Snead, O. C., and Gibson, K. M. (2009) Comparative genomics of aldehyde dehydrogenase 5a1 (succinate semialdehyde dehydrogenase) and accumulation of gamma-hydroxybutyrate associated with its deficiency. *Hum. Genomics* **3**, 106-120
10. Bouché, N., Fait, A., Bouchez, D., Møller, S. G., and Fromm, H. (2003) Mitochondrial succinic-semialdehyde dehydrogenase of the γ-aminobutyrate shunt is required to restrict levels of reactive oxygen intermediates in plants. *Proc. Natl. Acad. Sci. USA* **100**, 6843–6848
11. Toyokura, K., Watanabe, K., Oiwaka, A., Kusano, M., Tameshige, T., Tatematsu, K., Matsumoto, N., Tsugeki, R., Saito, K., and Okada, K. (2011) Succinic semialdehyde dehydrogenase is involved in the robust patterning of *Arabidopsis* leaves along the Adaxial–Abaxial axis. *Plant Cell Physiol.* **52**, 1340-1353
12. Schneider, B. L., and Reitzer, L. (2012) Pathway and enzyme redundancy in putrescine catabolism in *Escherichia coli*. *J. Bacteriol* **194**, 4080-4088
13. Steinhauser, D., Fernie, A. R., and Araújo, W. L. (2012) Unusual cyanobacterial TCA cycles: not broken just different. *Trends Plant Sci.* **17**, 503-509
14. Zhang, S., and Bryant, D. A. (2011) The tricarboxylic acid cycle in cyanobacteria. *Science* 334, 1551-1553

15. Kim, Y., Lee, S., Kwon, O., Park, S., Lee, S., Park, B., and Kim, K. (2009) Redox-switch modulation of human SSADH by dynamic catalytic loop. *EMBO J.* **28**, 959-968
16. Ahn, J. W., Kim, Y. G., and Kim, K. J. (2010) Crystal structure of non-redox regulated SSADH from *Escherichia coli*. *Biochem. Biophys. Res. Commun.* **392**, 106-111
17. Langendorf, C. G., Key, T. L., Fenalti, G., Kan, W. T., Buckle, A. M., Caradoc-Davies, T., Tuck, K. L., Law, R. H., and Whisstock, J. C. (2010) The x-ray crystal structure of *Escherichia coli* succinic semialdehyde dehydrogenase; structural insights into $NADP^+$/enzyme interactions. *PLoS One* **5**, e9280
18. Green, J., and Paget, M. S. (2004) Bacterial redox sensors. *Nat. Rev. Microbiol.* **2**, 954-966.
19. de Carvalho, L. P., Ling, Y., Shen, C., Warren, J. D., and Rhee, K. Y. (2011) On the chemical mechanism of succinic semialdehyde dehydrogenase (GabD1) from *Mycobacterium tuberculosis*. *Arch. Biochem. Biophys.* **509**, 90-99
20. Busch, K. B., and Fromm, H. (1999) Plant succinic semialdehyde dehydrogenase. Cloning, purification, localization in mitochondria, and regulation by adenine nucleotides. *Plant Physiol.* **121**, 589-597
21. Tsybovsky, Y., Donato, H., Krupenko, N. I., Davies, C., and Krupenko, S. A. (2007) Crystal structures of the carboxyl terminal domain of rat 10-formyltetrahydrofolate dehydrogenase: Implications for the catalytic mechanism of aldehyde dehydrogenases. *Biochemistry* **46**, 2917-2929
22. Gouet, P., Robert, X., and Courcelle, E. (2003) ESPript/ENDscript: extracting and rendering sequence and 3D information from atomic structures of proteins.

Nucleic Acids Res. **31**,3320-3323

23. Otwinowski, Z., and Minor, W. (1997) Processing of X-ray diffraction data collected in oscillation mode. *Methods Enzymol.* **276**, 307-326
24. Adams, P. D., Afonine, P. V., Bunkóczi, G., Chen, V. B., Davis, I. W., Echols, N., Headd, J. J., Hung, L. W., Kapral, G. J., Grosse-Kunstleve, R. W., McCoy, A. J., Moriarty, N. W., Oeffner, R., Read, R. J., Richardson, D. C., Richardson, J. S., Terwilliger, T. C., and Zwart, P. H. (2010) PHENIX: a comprehensive Python-based system for macromolecular structure solution. *Acta Crystallogr. D Biol. Crystallogr.* **66**, 213-221
25. Emsley, P., Lohkamp, B., Scott, W. G., and Cowtan, K. (2010) Features and development of Coot. *Acta Crystallogr. D Biol. Crystallogr.* **66**, 486-501
26. Winn, M. D., Ballard, C. C., Cowtan, K. D., Dodson, E. J., Emsley, P., Evans, P. R., Keegan, R. M., Krissinel, E. B., Leslie, A. G. W., McCoy, A., McNicholas, S. J., Murshudov, G. N., Pannu, N. S., Potterton, E. A., Powell, H. R., Read, R. J., Vaginc, A., and Wilsonc, W. S. (2011) Overview of the CCP4 suite and current developments. *Acta Crystallogr. D Biol. Crystallogr.* **67**, 235-242
27. Chen, V. B., Arendall, W. B. 3rd, Headd, J. J., Keedy, D. A., Immormino, R. M., Kapral, G. J., Murray, L. W., Richardson, J. S., and Richardson, D. C. (2010) MolProbity: all-atom structure validation for macromolecular crystallography. *Acta Crystallogr. D Biol. Crystallogr.* **66**, 12-21
28. Steinmetz, C. G., Xie, P., Weiner, H., and Hurley, T. D. (1997) Structure of mitochondrial aldehyde dehydrogenase: the genetic component of ethanol aversion. *Structure* **5**, 701-711
29. Wymore, T., Deerfield, D. W. II, and Hempel, J. (2007) Mechanistic

implications of the cysteine-nicotinamide adduct in aldehyde dehydrogenase based on quantum mechanical/molecular mechanical simulations. *Biochemistry* **46**, 9495-9506

30. Tsybovsky, Y., and Krupenko, S. A (2011) Conserved catalytic residues of the ALDH1L1 aldehyde dehydrogenase domain control binding and discharging of the coenzyme. *J. Biol. Chem.* **286**, 23357-23367
31. Holm, L., and Rosenström, P. (2010) Dali server: conservation mapping in 3D. *Nucleic Acids Res.* **38**, W545-W549
32. Muñoz-Clares, R. A., Díaz-Sánchez, A. G., González-Segura, L., and Montiel, C. (2010) Kinetic and structural features of beta aldehyde dehydrogenases: Mechanistic and regulatory implications. *Arch. Biochem. Biophys.* **493**, 71-81
33. Di Costanzo, L., Gomez, G. A., and Christianson, D. W. (2007) Crystal structure of lactaldehyde dehydrogenase from *Escherichia coli* and inferences regarding substrate and cofactor specificity. *J. Mol. Biol.* **366**, 481-493
34. Díaz-Sánchez, A. G., González-Segura, L., Rudiño-Piñera, E., Lira-Rocha, A., Torres-Larios, A., and Muñoz-Clares, R. A. (2011) Novel NADPH–cysteine covalent adduct found in the active site of an aldehyde dehydrogenase. *Biochem. J.* **439**, 443-452
35. Cheeseman, J. M. (2006) Hydrogen peroxide concentrations in leaves under natural conditions. *J. Exp. Bot.* **57**, 2435-2444
36. González-Flecha, B., and Demple, B. (1997) Homeostatic regulation of intracellular hydrogen peroxide concentration in aerobically growing *Escherichia coli*. *J. Bacteriol.* **179**, 382-388
37. Halliwell, B., Clement, M. V., and Long, L. H. (2000) Hydrogen peroxide in

the human body. *FEBS Lett.* **486**, 10-13

38. Salmeen, A., Andersen, J. N., Myers, M. P., Meng, T., Hinks, J. A., Tonks, N. K., and Barford, D. (2003) Redox regulation of protein tyrosine phosphatase 1B involves a sulphenyl-amide intermediate. *Nature* 423, 769-773

ABSTRACT IN KOREAN

해양미생물인 *Synechococcus*로부터 유래한 Succinic semialdehyde dehydrogenase (SySSADH)는 aldehyde dehydrogenase family에 속하는 효소로서 이 family에 속하는 효소들의 구조와 기능은 이미 잘 알려져 있으며 이 계열 효소들의 주된 기능은 기질의 aldehyde group을 carboxyl group으로 전환하는 것이다. 이들 상호간의 아미노산 1차 서열의 유사성은 적지만 전체적인 구조가 비슷하며 특히 Cysteine과 Glutamate로 이루어진 catalytic loop은 상당히 유사한 특징이 있다. 이런 SSADH 효소들은 γ-aminobutyrate shunt에서 γ-aminobutyrate의 분해 중간 산물인 succinic semialdehyde의 aldehyde group을 산화시켜 succinate를 생성하는 역할을 한다. 하지만 γ-aminobutyrate shunt에서 역할을 하는 다른 유래의 SSADH와는 달리 SySSADH는 2-oxoglutarate dehydrogenase 효소가 결핍되어 있다고 알려진 cyanobacteria의 TCA cycle에서 이 결핍을 우회하는 효소로서의 역할을 한다. SySSADH 효소는 $NADP^+$를 조효소로 사용하여 succinate를 생산하며 활성 부위에 2개의 Cysteine residue를 가진 다른 SSADH와는 달리 1개의 Cysteine을 가지고 있다. 이 논문에서 SySSADH의 구조, 조효소인 $NADP^+$, NADPH 그리고 기질인 Succinic semialdehyde가 결합된 총 3개의 구조를 규명하였으며 이 구조들을 통하여 조효소가 활성부위에 존재하는 Cysteine 잔기에 직접적으로 결합한다는 사실을 밝혔고 이러한 결합이 기질과 조효소의

반응으로 넘어가는 과정에서 thiohemiacetal 중간체로 연결되는 작용 기작을 입증하였다. 추가적인 분석으로 SySSADH는 산화에 민감한 효소로서 조효소인 NADP와 Cysteine의 결합이 과산화 수소의 산화 스트레스에서부터 효소의 활성을 보호하는 역할을 함을 확인하였다. 이러한 SySSADH의 구조적 기능적 특징은 2개의 Cysteine 잔기가 disulfide bridge의 redox를 통하여 산화를 방지하는 방식과는 달리 조효소를 통한 산화 방지 기작을 입증하였다.

주요어 ; Aldehyde dehydrogenase, Oxidation protection, Cofactor, Succinic semialdehyde dehydrogenase, *Synechococcus* sp. PCC 7002, tricarboxylic acid cycle

학 번 ; 2009-30309

ACKNOWLEDGMENTS

2003년, 지금의 지도교수님이신 이상기 선생님의 생화학 수업에서 본 단백질의 3차 구조에 매료된지 11년이 흘러 지금 박사학위를 마무리 짓는 단계에 섰습니다. 2003년 이후로 학부 졸업 실험생, 석사과정 그리고 박사과정에 이르기까지 결코 짧지 않은 그 긴 시간동안 꾸준한 지도와 가르침 그리고 보살핌을 주신 지도교수님이신 이상기 선생님께 항상 모자란 제자로써 뭐라 말씀드릴 수 없는 감사를 드립니다. 또한 저의 학문적 소양과 과학자로서의 자질을 기를 수 있게 도와주신 응용생명화학 전공교수님들이신 지금은 은퇴하신 김수일 교수님, 정진 교수님을 비롯하여 김수언 교수님, 최양도 교수님, 김정한 교수님, 노희명 교수님, 오기봉 교수님, 김민균 교수님, 신찬석 교수님, 배의영 교수님들께 감사드립니다. 그리고 1997년 응용생물화학부로 입학한 저에게 식물병리학과 관련한 많은 가르침을 주신 또다른 전공인 응용생물학 전공 교수님들이신 이인원 교수님, 황인규 교수님, 박은우 교수님께 감사드립니다. 또한 저의 첫 박사논문인 LFTase 효소의 기능 분석에 큰 도움을 주신 부산대학교 차재호 교수님과 그당시 대학원생이었던 박영돈 학우에게도 감사의 말을 전하고 싶습니다. 그리고 저의 박사학위 논문 심사를 위해 강릉에서 먼길임에도 불구하고 참석하셔서 많은 조언을 아끼지 않으신 강릉 KIST 판철호 박사님께도 다시 한번 감사드립니다.

석사 그리고 박사... 그 긴 기간동안 여러가지 어려움과 고민들을 해결하는데 구조생물학실 식구들의 도움이 참 컸던 것 같습니다. 처음 석사과정에 입학했을 때 사수로 여러가지 실험을 가르쳐준 박사 정우석형과 정두교형, 함께 석사과정을 함께 동고동락했던 이수진과 이지현, 그리고 지금도 박사과정으로 함께 있는 박양신, 박사과정을 시작할 때 많은 도움을 준 박사 김명일형, 항상 실험과 관련하여 언제나 논의 상대가 되어준 지금은 졸업한 박사 조장희형을 포함한 지금도 함께하고 있는 신인철형, 유상헌, 오준택, 김상훈과 졸업한 정지웅, 조수희와 한기태, 이 모든 사람들과 함께한 시간에 감사합니다.

그리고 그동안 전 참 못난 아들이자 동생이자 사위이자 남편이었던 것 같습니다. 대학졸업도 모자라 대학원에 진학하겠다고, 잘 다니던 직장도 그만두고 박사과정에 진학하겠다고 했을 때, 저의 의견을 존중해주시고 묵묵히 뒤에서 지원해주시는 어머니와 작고하신 아버지, 그리고 항상 챙겨주는 큰형 진태형과 작은형 진호형, 보잘것없는 저에게 흔쾌히 사랑하는 딸과의 결혼을 허락하시고 수시때때로 보살펴 주시는 장인어른과 장모님 그리고 손위처남 오승 형님께 감사드립니다.

마지막으로 11년간 한마디 불평불만 없이 과거에는 애인으로 이제는 저의 아내가 되어 저를 지켜봐주고 항상 정신적 버팀목이 되어주어 너무나 미안하고 사랑하는 나의 아내, 오수연에게 이 논문을 바칩니다.